School of Science and Engineering

Physics

The Decay of X-ray Emission From Young star's

Jacob Sterling

PH40006 BSc Physics with Astrophysics Project Report

Academic year: 2020-2021

Supervisor: Dr Scott G. Gregory

University of Dundee

Declaration of authorship

The following work has been completed by Jacob Sterling and is wholly my own work, unless stated otherwise. It has not been submitted for assessment elsewhere and I have not knowingly allowed it to be used or copied by any other person. I confirm that I have read and understood the School policy on Academic Dishonesty.

Candidate's signature: Jacob Sterling Date: 14th May 2020

Contents

ABSTRACT

The observed X-ray luminosity of young or otherwise known as pre-main sequence (PMS) star's, decreases with age as they evolve across the Hertzprung-Russel Diagram towards the main sequence. The origin of a star's X-ray luminosity that is known to be majorly due to the X-ray emissions from the star's X-ray emitting plasma that forms along the field lines of the stellar magnetic field known as the stellar corona. The star's magnetic field is generated by the configuration of the stellar interior, PMS star's with fully-convective interiors are observed to have relatively simple magnetic fields and larger X-ray luminosity compared to PMS star's with a radiative core that have more complex magnetic Fields and smaller X-ray luminosity. The work done in this paper explored the relationship between a typical PMS star's X-ray luminosity with an increase in magnetic field complexity and explains the observed "decay" of the X-ray luminosity with age in PMS star's.

1 Introduction

Pre-main sequence (PMS) star's or T Tauri star's are star's that have not yet reached the main sequence. The are still evolving across the Hertzsprung-Russel (HR) diagram as they contract under gravity. When the stellar winds clear away their natal clouds of dust, the PMS star's emerge and are first visible at optical wavelengths and lie along the stellar birth line in the HR diagram (Stahler 1983). the birth line is represented in Figure 1.1 by the top right most diagonal dotted line. The dashed lines represent the PMS star's evolution tracks for different masses, through the PMS towards the zero-age main sequence (ZAMS) of the HR-diagram (Larson 2003). PMS star's at the birthline typically have acquired nearly all of their mass but have not begun nuclear fusion (Davies 2015). Lower mass PMS star's typically host fully convective interiors. Subject to the virial theorem, as the star contracts under its own gravitational force (gravitational contraction), half of this gravitational energy heats the stellar interior while the other half is radiated away (Gregory et al. 2016). The stellar radius decreases with increasing age as $R_* \propto t^{-1/3}$. For star's $\gtrsim 0.35M_\odot$, the opacity in the core drops with

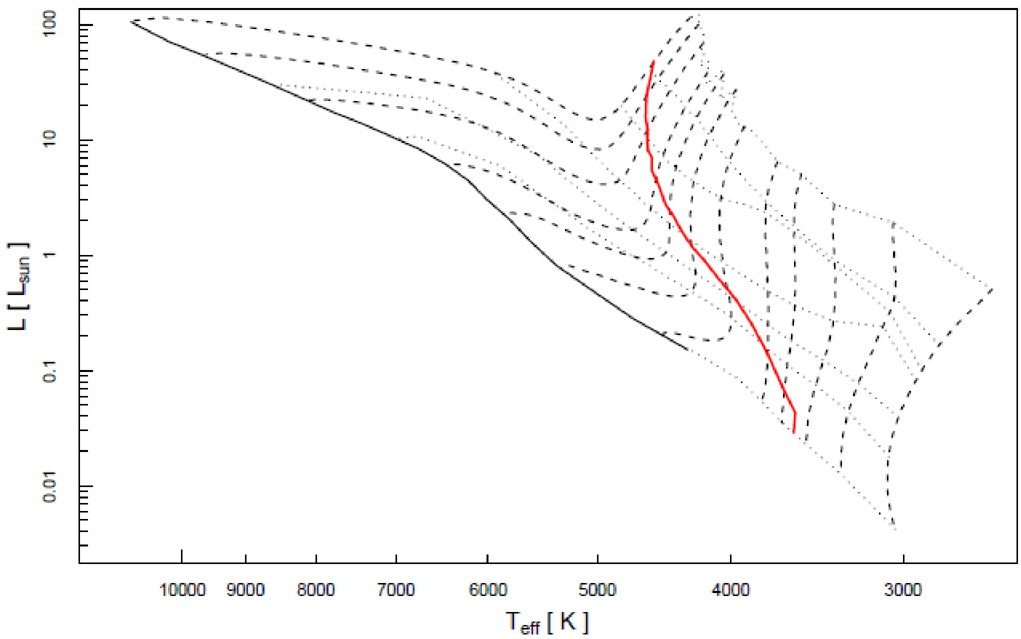

Figure 1.1: The PMS of the HR diagram with only birth line, zero age main sequence (ZAMS) and evolution tracks for PMS star's generated from Siess et al. (2000) models (Davies 2015). Dashed lines from right to left correspond to mass tracks of 0.1, 0.2, 0.3, 0.4, 0.5, 0.75, 1.0, 1.25, and 3 $M_\odot$. The horizontal dotted lines illustrate the position of PMS star's by age (from top right downwards, the dotted lines are isochrones for 0.01, 0.2, 5, 10 and 60 Myr.). The solid black line represents the ZAMS. The solid red line marks the boundary between fully convective PMS star's (found on the right hand side of the line) and those that have formed radiative core (Gregory et al. 2014).

increasing temperature and eventually convection switches off in the central regions and the radiative core begins to grow. During this time the luminosity towards the center of the star will increase and will cause a decrease in the visible luminosity of the star's surface (Gregory et al. 2016), Following radiative core growth the luminosity eventually stop decreasing, and then will begin to increase along with the star's effective temperature along the mass tracks in the HR diagram (Gregory et al. 2016).

Classical T Tauri star's (CTTSs) have peculiar properties such as a strong flux in the emission lines up to 100% of the intrinsic luminosity of the star, complex magnetic activity, photometric variability and jets (Muzerolle et al. 2001). These peculiarity's can be explained by accretion. Accretion is the influx of mass from the remaining natal clouds of dust, low mass star's always form forms a surrounding 'accretion disk' from the remaining dust, which is seen less commonly in solar type and high mass star's. Weak lined T Tauri star's (WTTS) are non-accreting star's with thin accretion disks (Muzerolle et al. 2001). CTTSs are accreting star's that are actively accreting hot gas from their much larger surrounding accretion disk which manifests itself by strong emission lines in their spectrum. The mentioned emission lines (strong flux) actually form as the accreted gas hits the 'surface' of the star, Gregory et al. (2006) demonstrated that the magnetic field geometry has a significant effect in controlling the location and distribution of hotspots that arise from high velocity accreting material hitting the star(Stassun et al. 2006). The hotspots in accreting PMS star's emit soft X-rays that contribute a relatively small amount to the X-ray emission of the star compared to the X-ray emission from the corona. PMS star X-ray light curves consists of a 'quiescent' level of X-ray emission (L_X). Superimposed on the 'quiescent' emission are flares with much higher energy with the same temporal behavior as flares from the solar corona. The quiescent X-ray emission may be due to the superposition of emission from many smaller (unresolved) flares (Stassun et al. 2006). This coronal X-ray emission from hot ($\gtrsim 10MK$) plasma, arising from magnetic activity is the dominant source of PMS star X-ray emission.

A star's position in the HR diagram can give a general indication as to what stage of stellar evolution. Star's would generally follow a given path depending their mass heading towards the ZAMS. These "paths" are known as evolution tracks and an example of such is shown in figure 1.2. Solar mass star's ($M_* \sim M_\odot$) evolve can down what is known as the Hayashi track which is illustrated in Figure 1.2 and 1.1, where its luminosity decreases with increasing age, it then evolves onto the Henyey track where its luminosity increases within increasing age. Star's on the Henyey track have already developed substantial radiative cores (Gregory et al. 2016).We can use the Hayashi and Henyey tracks to categorise PMS star's by stellar interior, using this information we can make a few generalisations about the mass ranges found in figure 1.1). The first generalisation is for the evolution tracks with no Henyey track otherwise seen in figure

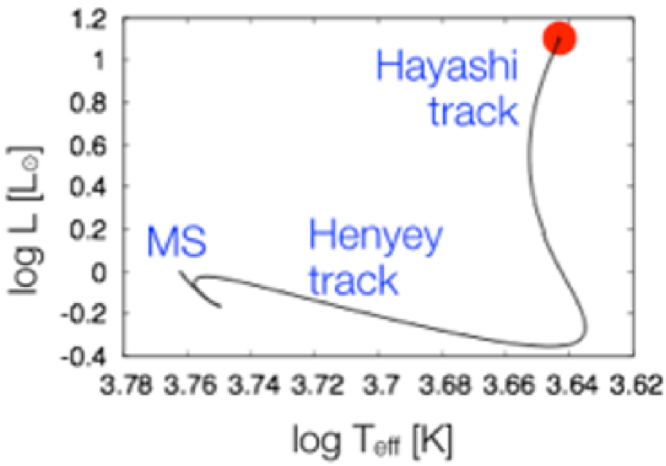

Figure 1.2: Close up representation for Hayashi and Henyey tracks in the HR diagram for 1 solar mass ($1M_{\odot}$) star. The Horizontal line represents the Henyey track while most of the vertical line represents the Hayashi track. MS denotes main sequence.

1.1) as the vertical dotted lines with no transformation into a horizontal line or interception with solid red line, meaning we can assume that no radiative core ever develops for star's along these evolution tracks (referring to a mass range 0.1 to 0.35 solar masses in 1.1)) and so do not evolve onto a Henyey track. The next generalisation is for evolution tracks with no Hayashi or red line interception, we can say for these that they developed their radiative cores before they were even visible at optical wavelengths on the HR-diagram (before the birth line), this does not apply to Figure 1.1 since they all have Hayashi tracks. Depending on the PMS star's interior format it can host different magnetic field configurations with varied complexity based on age and mass (Gregory et al. 2014).

According to stellar dynamo theory, magnetic fields (**B**-field) are generated by the circulation of the convective zone within the star. The motion of the conductive plasma within a star's interior acts like a dynamo, generating a magnetic field around the star which erupts through the stellar surface (Piddington 1983). The stellar magnetic field is affected by the pressure from its radiative core that produces force outwards towards the surface of the star counteracting the gravitational contraction enough to prevent the star from collapsing in on itself (Chabrier & Baraffe 1997). The dynamo mechanism changes from a fully convective one to one where there is a shear layer at the interface of the inner radiative zone and the outer convective envelope as PMS stars evolve across the HR diagram. This dynamo mechanism is then more similar to that of the solar dynamo. The magnetic field is generated at the internal shear layer (known as the tachocline in the Sun (Piddington 1983)).

We observe a difference in magnetic field configuration's when comparing PMS star's found on the Hayashi track compared to star's along the Henyey track (alternatively interpreted as a difference in **B**-fields for star's with radiative cores vs star's with only fully convective interiors) (Adams & Gregory 2012). As a PMS star's radiative core forms towards the end of the Hayashi track, a noticeable change in the configuration of the stellar magnetic field is observed to occur with the age of the star. The magnetic field becomes more complex, multipolar, and dominantly non-axisymmetric once a substantial radiative core has developed (Gregory et al. 2014).

A star's magnetic field can be also be effected by differential rotation of star causing highly concentrated magnetic fields. These concentrated **B**-fields become "wrapped" or "stretched" along the surface due to the differential rotation of the star (Piddington 1983). This magnetic activity can inhibit the circular convection of the star's interior creating areas of relatively low temperature areas known as 'star'spots' (or 'sunspots' on the Sun). Commonly formed above star'spots are a phenomenon termed as coronal loops which are magnetic loops from the star's surface hosting hot plasma along the loop from the interior that can heat the stellar corona to well over 10 million Kelvin (Hudson & Kosugi 1999). Such coronal loops create a X-ray emitting volume enclosed by the magnetic loop and star's surface, giving origin to a star's X-ray luminosity denoted L_X (Gregory et al. 2014).

The emission of X-rays from PMS star's is thought to arise from a scaled up version of the solar corona, where the star's bolometric luminosity, flares and mainly coronal loops contribute to the star's X-ray emission. Flares are the result of the twisting and tangling of magnetic loops due to footpoint motions on the stellar surface (Güdel 2009). This stores up magnetic energy which is released via magnetic reconnection, that accelerates particles along the loops generating X-ray emission (L_X). Flares can vary the measured L_X from a PMS star over relatively short time scales $\sim$ hours to days (Favata et al. 2005). A star's coronal magnetic loops contain the hot x-ray emitting plasma, the maximum radial extent of the star's corona can be estimated using a pressure balance argument (Jardine et al. 2002; Johnstone et al. 2014) Coronal magnetic loops can contain the hot plasma as long as the gas pressure does not exceed the magnetic pressure. Larger coronal loops are ripped away from the star by stellar winds as the magetic pressure from the star that holds the hot plasma naturally decreases with distance from the stellar surface leaving only the smaller more compact coronal loops that are what contribute to the overall X-ray emitting volume (Güdel 2009).The corona of PMS star's generally (mass $\gtrsim 0.35M_\odot$ and $\lesssim 3M_\odot$) can be $\sim 10 - 10^5$ times more X-ray luminous than the solar corona and up to ~ 15 times hotter (Gregory et al. 2016).

There exists X-ray wavelength signatures belonging to the presence of a radiative core, we can use these signatures to catagorise stars by stellar interior (seperate fully-convective stars) (Gregory et al. 2016). The observed X-ray luminosity decays rapidly once a radiative core grows, and particularly once stars evolve onto Henyey tracks. In this project work i explore wether the observed **B**-field complexity increase is linked to the X-ray luminosity decay, by developing models of coronal X-ray emission for multipolar magnetic fields. As PMS star's develop their radiative cores their **B**-fields become more complex hosting many more magnetic loops within their corona. Star's with simple fields are able to contain the X-ray emitting plasma to larger radii, therefore creating a bigger X-ray emitting volume and larger X-ray luminosity. The increase in magnetic field complexity causes the feilds influence **B** to decay faster with height above the star (Gregory et al. 2016), such complex fields are easier to pull open, therefore more compact and smaller X-ray emitting volume and X-ray luminosity. Higher mass PMS star's ($\gtrsim 3M_{\odot}$) develop their radiative cores faster than lower mass star's and have generally already developed their core by the time they become optically visible (Gregory et al. 2016) and so would be hard to gather representative data set for. Lower mass PMS star's of mass $\lesssim 0.35M_{\odot}$ generally host fully convective interiors even after reaching the main sequence and so would have relatively unchanging **B**-fields (Gregory et al. 2014). And so Solar type star's are the focus of observation to find a decay in X-ray emission with age.

In section §2.1 i describe the PMS magnetic evolution in more detail followed by §2.2 where i show how the X-ray emission links to an increase in magnetic field complexity through a series of equations that were used in my code to analyse magnetic models shown in section §3.1. §5 shows my calculated results of the X-ray luminosity for each model and shows how they change with increasing field complexity. Section §6 discusses my results and any further work i have done or could have done for my project.

2 Magnetic and X-ray Luminosity evolution

2.1 PMS star magnetic field evolution

Stellar magnetic fields are currently able to be mapped using two methods, Zeeman-Doppler Imaging (ZDI) and Magnetic Doppler imaging (MDI). ZDI reconstructs the 2D distribution of magnetic polarities across the surface of star's, determined by maximum entropy image reconstruction techniques (Donati et al. 1997). ZDI is responsible for the first successful magnetic maps of star's other than the sun (Donati et al. 2007) examples of which can be seen in Figure 2.1. Yet the resolution of magnetic surface maps produced by the ZDI method is limited by stellar rotation period and inclination making observation of smaller scale fields difficult, studies into stellar magnetism recently have made significant advances using optical spectropolarimeters which could lead to more refined magnetic surface maps (Donati et al. 1997). The MDI method uses polarised radiative transfer and linear polarisation diagnostics for **B**-field construction (Donati et al. 1997). Observations used by MDI is limited to the brightest and most magnetic star's, but is sure to see development (Donati et al. 1997).

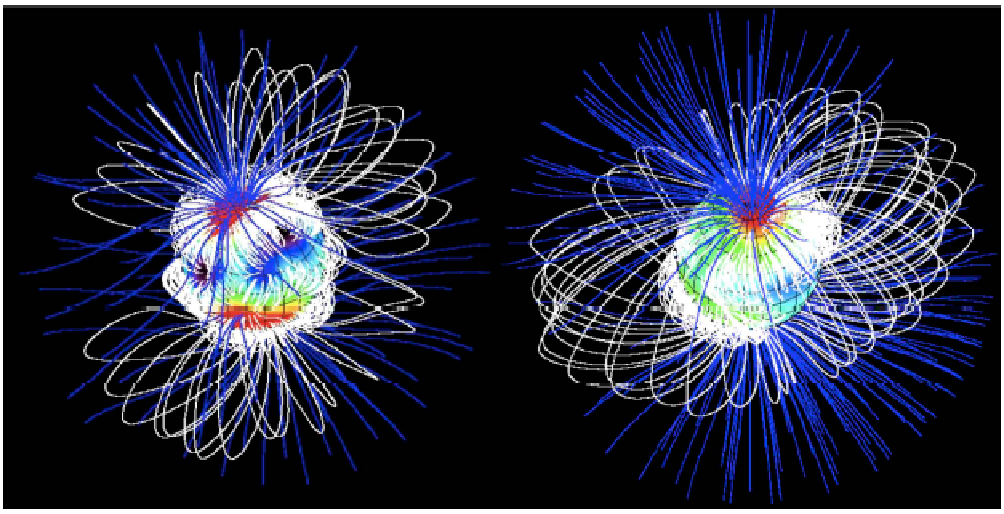
l

Figure 2.1: 3D field extrapolations constructed from Zeeman Doppler Imaging (ZDI) magnetic maps of the accreting T Tauri star's V2129 Oph and BP Tau (left and right respectively). Blue coloured lines represent the open field lines. White field lines represent the closed **B**-field lines and are the ones that contain the X-ray emitting plasma. Image from: (Gregory et al. 2010)

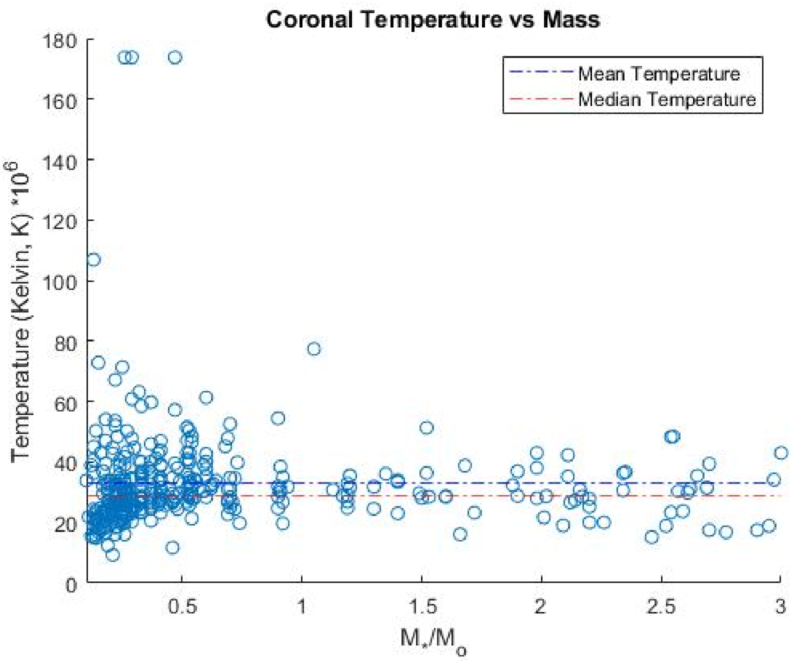

Figure 2.2: COUP data showing average PMS star coronal temperature for masses $0.1-3M_{\odot}$. The mean temperature of 3.3×10^7 K with a median absolute deviation (MAD) of $\pm 3.3 \times 10^3$ K (Getman et al. 2005)

Figure 2.5 is the PMS of the HR diagram split into sections based on the observed magnetic field topology of the star's found in that that region. The figure shows that as a star moves down its evolution tracks (vertical black lines and joint red curved lines) it will pass through the zones that demonstrates the star's evolution in magnetic field topology with age, or more specifically the star's change in field topology as it transitions from its Hayashi track to Henyey track.

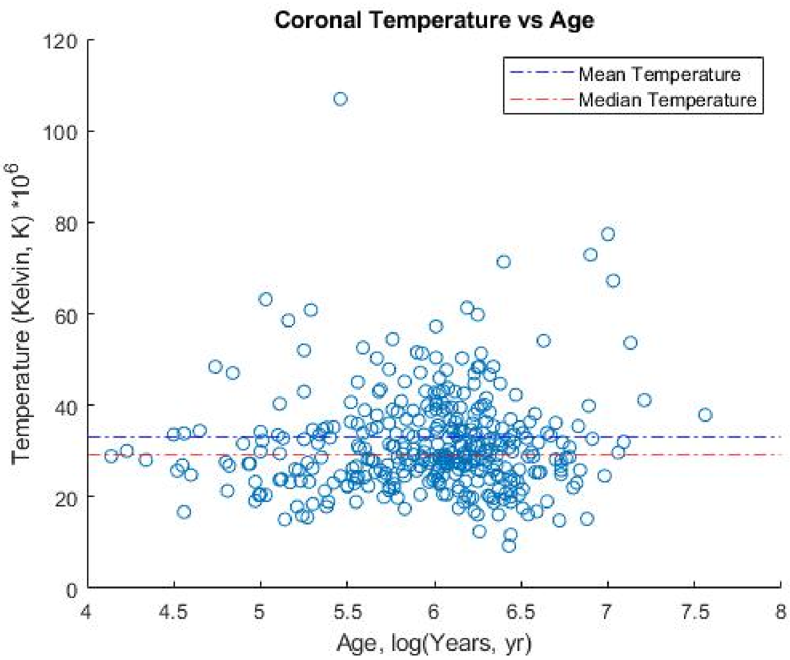

Figure 2.3: COUP data showing relationship between coronal temperature and increasing age (Getman et al. 2005).

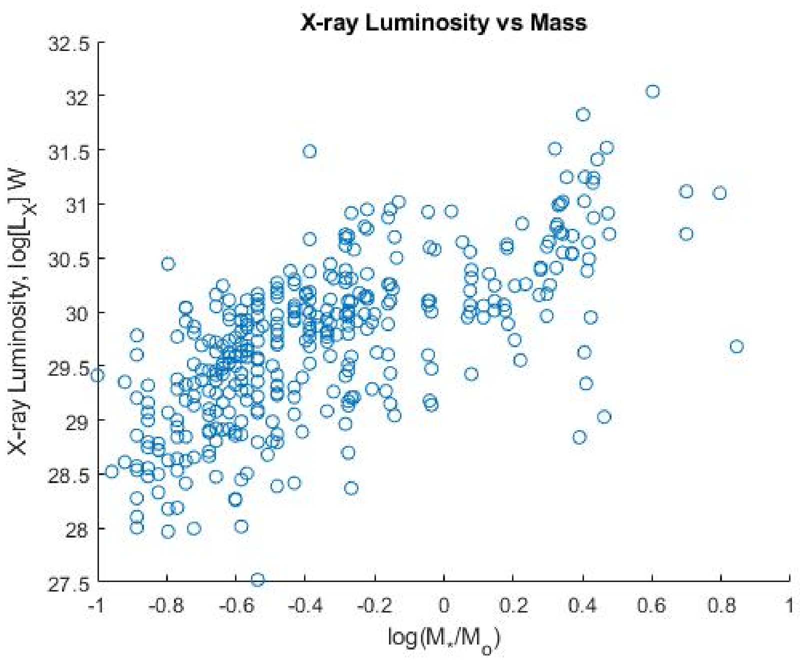

Figure 2.4: COUP data showing relationship between observed X-ray luminosity and increasing mass(Getman et al. 2005).

The magnetic maps of the three PMS star's in Figure 2.5 decrease in **B**-field complexity from 1 to 3 between the birth-line and ZAMS on the HR diagram. This increase in magnetic field complexity with age can be explained by the formation of the star's radiative core and its effect of the star's field topology and the associated change in the stars magnetic dynamo magnetic

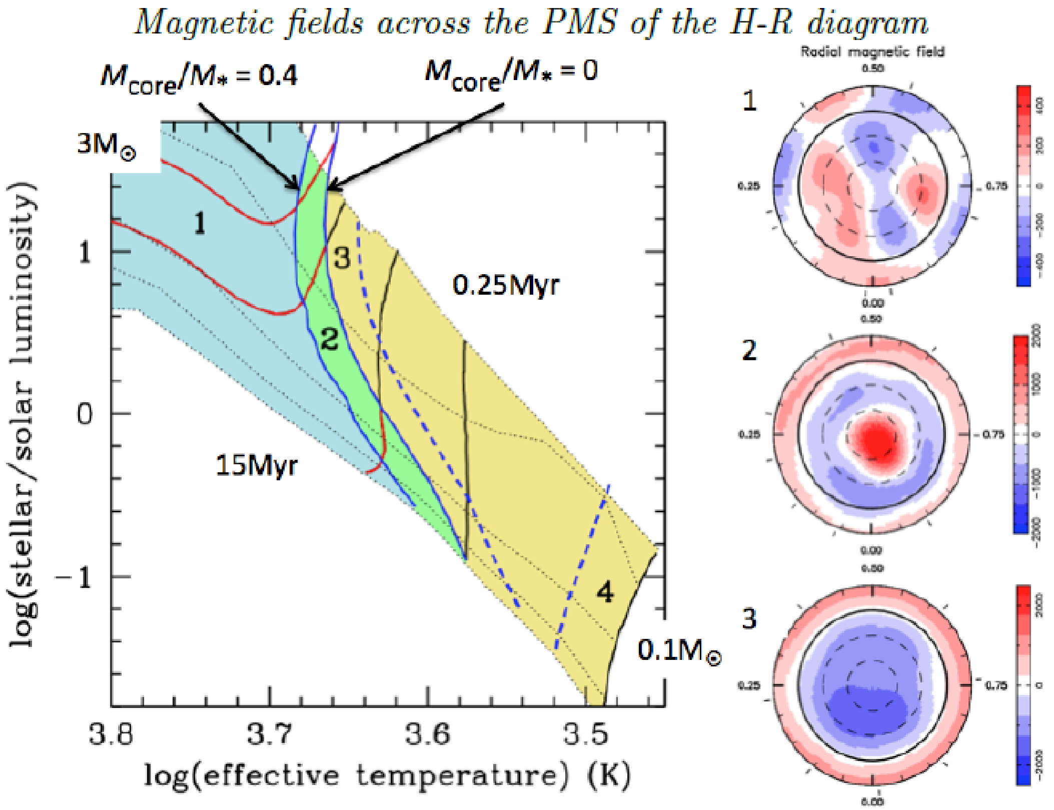

Figure 2.5: Magnetic HR diagram. The PMS is shown with mass tracks colored as solid red and black (showing from right to left respectively, 0.1, 0.5, 1, 2 and 3 $M_\odot$). Dotted black lines indicate ages (from top right down as 0.25, 1, 5, 10 and 15 Myr). The magnetic maps shown on the right of the figure are for star's with different stellar interiors and correspond to the numbered regions on the diagram to which they belong. The solid blue lines show the boundaries of region 2 and the dashed blue lines indicate the upper and lower boundary between region 3 and 4. star's in region 1 are largely radiative with complex non-axisymmetric large scale magnetic fields. star's in region 2 have small radiative cores and axisymmetric magnetic fields that are typically dominantly octupolar. star's in region 3 are fully convective with axisymmetric and dominant dipole magnetic fields. The lowest mass fully convective PMS star's in region 4 are speculated to host a variety of large scale magnetic field configurations yet to be discovered. Figure from (Gregory et al. 2014)

field generation process. Gregory et al. (2016) supports this theory, providing evidence of X-ray wavelength signatures belonging to the presence of a radiative core. Gregory et al. (2016) compares the X-ray luminosity of star's with a radiative core to star's with fully convective interiors. Observations show the X-ray contribution to the star's total luminosity in star's with radiative cores have a lower mean compared to those with fully-convective interiors. This suggests that the observed increase in magnetic field complexity, and the observed decay in X-ray luminosity may be linked.

2.2 Evolution of X-ray emission

Typical observed X-ray luminosity's and temperatures for PMS star's seen in the Figures 2.6, 2.7, 2.8, 2.9, 2.2 and **??**, from X-ray observations and source lists from the Chandra Orion Ultradeep Project (COUP). The COUP data set catalogued more than 1600 X-ray point sources from the exceptionally deep 2003 January Chandra X-Ray Observatory (Chandra) observation of the Orion Nebula Cluster and embedded populations around OMC-1 (Getman et al. 2005), the OMC-1 is a well studied star forming region. The COUP data contains observations of young star's under 10 Myrs of age, Figure 1.1 suggests these would be majority Hayashi track PMS star's and so we should see a decrease in X-ray luminosity with increasing age towards the Henyey track.

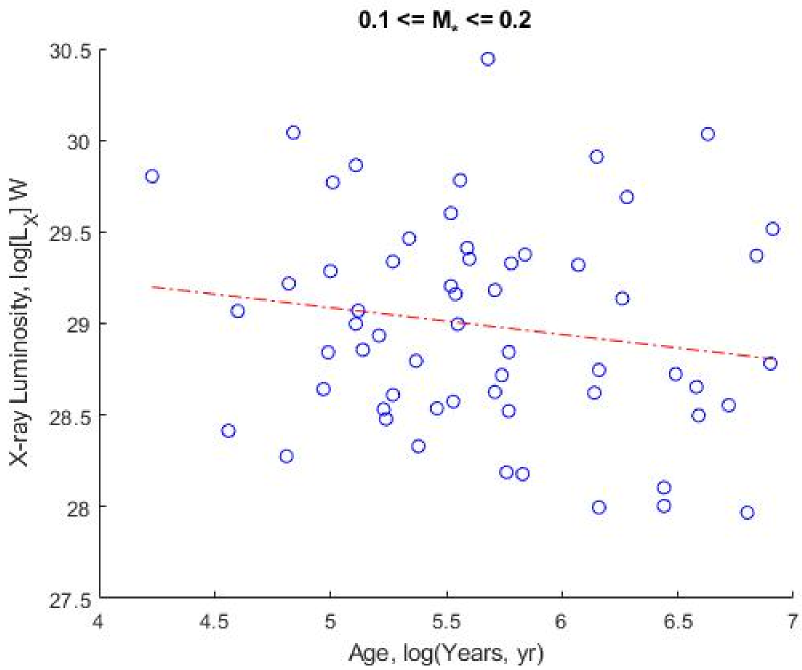

Figure 2.6: COUP data showing relationship between observed X-ray luminosity and increasing age for stars of mass $0.1 <= \frac{M_*}{M_\odot} <= 0.2$ (Getman et al. 2005). Red line represents a calculated least squares fit describing trend in data.

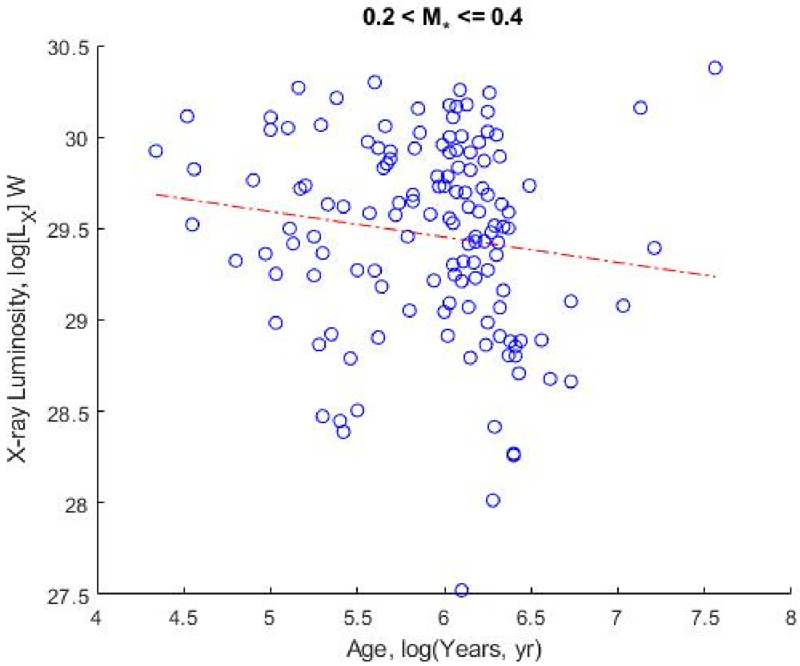

Figure 2.7: COUP data showing relationship between observed X-ray luminosity and increasing age for stars of mass $0.2 < \frac{M_*}{M_\odot} <= 0.4$ (Getman et al. 2005). Red line represents a calculated least squares fit describing trend in data.

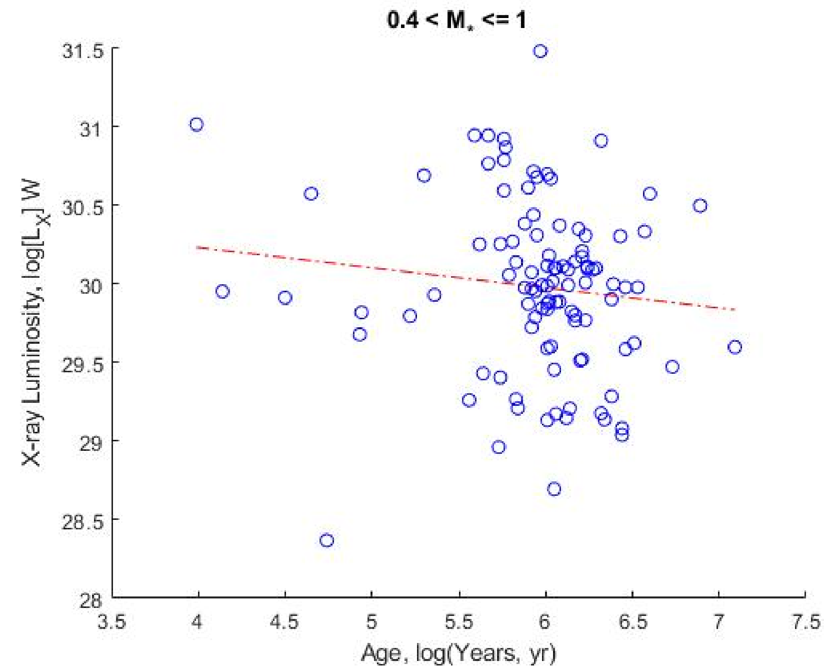

Figure 2.8: COUP data showing relationship between observed X-ray luminosity and increasing age for stars of mass $0.4 < \frac{M_*}{M_\odot} <= 1$ (Getman et al. 2005). Red line represents a calculated least squares fit describing trend in data.

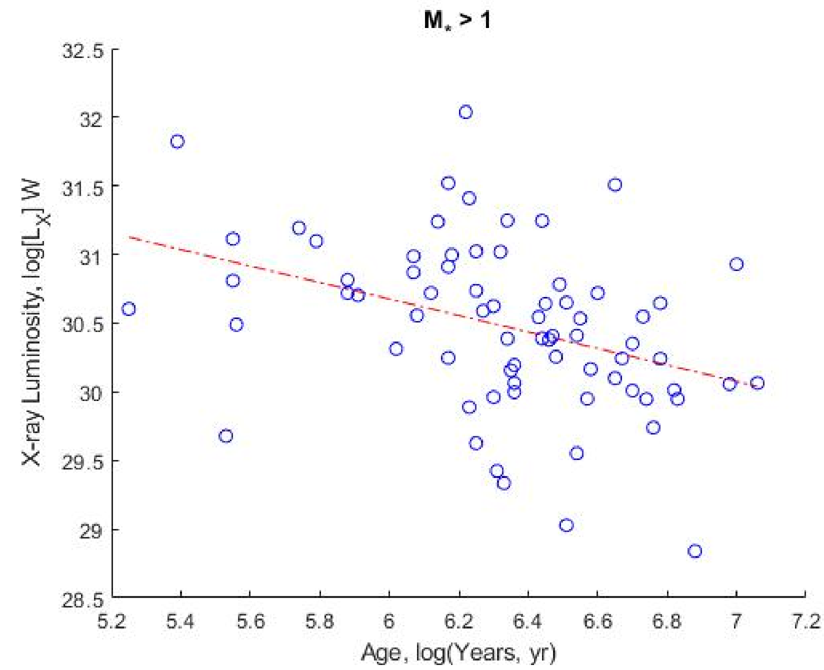

Figure 2.9: COUP data showing relationship between observed X-ray luminosity and increasing age for stars of mass $\frac{M_*}{M_\odot} > 1$ (Getman et al. 2005). Red line represents a calculated least squares fit describing trend in data.

Despite the many outliers in Figures 2.6, 2.7, 2.8 and 2.9 there is a slight negative correlation between the star's X-ray luminosity and age which is as we would expect in Hayashi track star's of given mass ranges. We would not see the any corralation close to the ones seen in these figures compared to a L_X vs Age graph of all masses , this could be explained by L_X's relationship with mass seen in Figure 1.1. Figure **??** and **??** show the X-ray luminosity's correlation with mass and coronal temperature. Figure 2.4 shows a very clear increase in a star's observed X-ray luminosity with increasing mass.

The goal of my project is to demonstrate if the increase in magnetic field complexity as PMS star's age is linked to the observed decrease in X-ray luminosity. Gregory et al. (2014) and Folsom et al. (2016) argue that the magnetic properties of PMS star's are related to their positions in the HR-Diagram. It was found that as a PMS star evolves towards the main sequence (increasing age), its stellar interior structure is subject to change that influences its magnetic field properties. The focus of my project work is on the change in complexity of the magnetic field and how this effects the change in X-ray luminosity. The coronal X-ray luminosity depends on the enclosed volume of the coronal plasma enclosed by the star's magnetic field (Güdel 2009). The mentioned X-ray Luminosity (L_X) is related to the enclosed X-ray emitting volume V via (Güdel 2009):

$$L_X \approx \Lambda(T_X)\varepsilon_M = \iiint_V \Lambda(T_X) n^2 dV \tag{1}$$

where $\Lambda(T_X)$ represents the radiative loss function which is a piecewise function of the coronal temperature T_X, n is the coronal density, and ε_M is the emission measure which is used to evaluate the X-ray luminosity analytically in my project work. The Radiative loss function $\Lambda(T_X)$ may be expressed as (Aschwanden et al. 2008),

$$\Lambda(T_X) = \begin{cases} 10^{-21.94}, & 10^{5.75}K < T_X < 10^{6.3}K \\ 10^{-17.73}T_X^{-2/3}, & 10^{6.3}K < T_X < 10^{7.3}K \\ 10^{-24.66}T_X^{1/4}, & T_X > 10^{7.3}K \end{cases} \tag{2}$$

For a given coronal temperature T_X the radiative loss function gives a value as long as the coronal temperature is above a value of $10^{5.75}$ K and only for temperature values above $10^{6.3}$ K does the the value depend more specifically on the coronal temperature T_X (Aschwanden et al. 2008). To fully determine the emission measure ε_M, a few mentioned parameters and dimensionless quantity's in the above equations are defined as shown in Table 2.1 and below (Adams & Gregory 2012) where r is the radial distance from the star's surface:

$$\Phi_g \equiv \frac{GM_*}{R_* c_s^2}, \quad \Phi_c \equiv \frac{1}{2}\left(\frac{\omega R_*}{c_s}\right)^2, \quad \text{and} \quad \xi \equiv \frac{r}{R_*}. \tag{3}$$

Assuming an isothermal corona and that the corona is in hydrostatic equilibrium we can calculate the sound speed (c_s) through the plasma with the ideal gas law.

$$c_s^2 = \left(\frac{k_B T_X}{\mu m_H}\right) \tag{4}$$

μ is the mean molecular weight, m_H is the mass of a hydrogen atom, k_B and T_X are defined in Table 2.2 and 2.1. ω is the rotation rate equal to $2\pi/P_{rot}$, where P_{rot} is the star's rotation period in seconds. B_θ/B_r in equation 15 is the ratio of the components of the stellar magnetic field (assuming an axisymetric magnetic field with $B_\phi = 0$) in the thetal and radial direction described by equation 19 in the next section. Equation 1 shows the X-ray luminosity's dependence on the emission measure or enclosed X-ray emitting volume V. I found the most viable way to measure L_X was to analytically determine the emission measure where the coronal emission depends on the number density n of the coronal plasma, which depends on the pressure P,

$$n = \frac{P}{2k_B T_X} \tag{5}$$

And so the emission measure in equation 1 is expressed as,

$$\varepsilon_M = \frac{R_*^3 P_0^2}{4(k_B T_X)^2} E \tag{6}$$

Where,

$$E \equiv \int_V (P/P_0)^2 \pi \xi^2 d\xi d\mu \tag{7}$$

And P is the gas pressure at radial distance r from the surface of the star and at angle theta from the set pole. We can calculate the pressure at any point along a magnetic loop by assuming the plasma along the the loop is isothermal and in hydrostatic equalilbrium (Gregory et al. 2006), in this case,

$$P(s) = P_0 \exp\left[\frac{1}{c_s^2}\int g \cdot \hat{s} ds\right] \tag{8}$$

where the integral starts at the stellar surface and continues to the point s along the magnetic loop where,

$$\mathbf{g} \cdot \hat{\mathbf{s}}\ ds = \frac{1}{B} g \cdot \mathbf{B} ds = g_r dr + \frac{B_\theta}{B_r} g_\theta dr. \tag{9}$$

The Pressure integral 8 then becomes,

$$P(s) = P_0 \exp\left[\frac{1}{c_s^2}\left(\int_{R_*}^{r} g_r dr + \int_{R_*}^{r} \frac{B_\theta}{B_r} g_\theta dr\right)\right] \tag{10}$$

In order to determine the pressure, we must evaluate the integrals,

$$I_1 = \frac{1}{c_s^2}\int_{R_*}^{r}\left(-\frac{GM_*}{r^2}\right) dr = \frac{GM_*}{c_s^2 R_*}\left(\frac{R_*}{r} - 1\right), \tag{11}$$

$$I_2 = \frac{1}{c_s^2}\int_{R_*}^{r} \omega^2 r \sin^2\theta dr, \tag{12}$$

$$I_3 = \frac{1}{c_s^2}\int_{R_*}^{r} \frac{B_\theta}{B_r}\omega^2 \sin\theta\cos\theta dr. \tag{13}$$

Then using the dimensionless quantities from equation 3 the integrals can be written as,

$$I_1 = \phi_g\left(\frac{1}{\xi} - 1\right) \tag{14}$$

so that I_1 is the same for all magnetic field configurations,

$$I_2 = \phi_c J_2 \quad \text{where} \quad J_2 = 2\int_1^{\xi} \sin\theta^2 \xi d\xi, \tag{15}$$

$$I_3 = \phi_c J_3 \quad \text{where} \quad J_3 = 2\int_1^{\xi} \frac{B_\theta}{B_r}\sin\theta\cos\theta\xi d\xi. \tag{16}$$

Which means we must evaluate J_2 and J_3 for various magnetic field configurations. Along each field line the angle θ depends on the dimensionless constant ξ, which is determined by the field geometry. The gas pressure can then be written as,

$$P = P_0 \exp\left[\Phi_g\left(\frac{1}{\xi} - 1\right) + \Phi_c(J_2 + J_3)\right] \tag{17}$$

P_0 is the gas pressure at the foot points at the magnetic loop being considered within the stellar corona. If we then assume that the gas pressure at the base is proportional to the magnetic pressure (Jardine et al. 2002) then $P_0 = KB_0^2$ where K is a proportionality parameter that can be seen for dipole + octupole field configurations in Table 4.2 such field configurations are typical for many Hayashi track PMS stars. For the purpose of presentable data a proportionality constant of $10^{-5.0}$ is used for pure multipolar models and $10^{-6.8}$ for combination multipolar (more than one field component) (Johnstone et al. 2014). J_3 in equation 15 depends on the B_θ/B_r ratio defined by equation 19 in section §3.1 which when used for very small values of B_r (found at the apex of larger magnetic field loops or at the null point explained in detail in section §4) would cause J_3 to become very large which can cause analytical problems.

Parameter	Description	Units
R_*	stellar radius	centimeters, cm
K	proportionality constant (Jardine et al. 2002)	N/A
T_X	coronal temperature	Kelvin, K
B_*	magnetic field strength	Gauss, G
M_*	stellar mass	Solar Masses, $M_\odot$
w	rotation rate	radians per second, rad^{-1}
ℓ	field configuration	N/A

Table 2.1: Table showing all relevant stellar parameters to evaluation accompanied by their mathematical units.

Constant	Description	Units
k_B	Boltzmann constant	$erg.K^{-1}$
G	gravitational constant	$cm^3g^{-1}s^{-2}$
μ	mean molecular weight	u
m_H	mass of hydrogen atom	grams

Table 2.2: Table showing all relevant constants to evaluation accompanied by their mathematical units.

3 Models of stellar magnetic fields

3.1 Axisymmetric multipoles

The X-ray luminosity for a given set of stellar parameters; magnetic field strength, radius, mass, rotational period, coronal temperature, proportionality constant (Jardine et al. 2002) and the assumed field configuration shown in Table 2.1. If the star has a multi-polar combination field configuration the field strength of each field component must be given; for example, dipole + octupole field configurations shown in Table 4.2 (and star 1 in figure 2.5) have magnetic field strength components B_{dip} and B_{oct}, Donati et al. (2011) shows observed values of ratio B_{dip}/B_{oct}. A star's field topology would have to be determined after analysing magnetic surface maps generated by ZDI or MDI mentioned in section §2.1, to gather its ℓ number or numbers depending on its complexity ($\ell = 1$ corresponds to a dipole, $\ell = 2$ a quadrupole, $\ell = 3$ a octupole etc.). The magnetic field strength B_* at any point within the star's magnetic field would depend on its magnetic field configuration. Gregory et al. (2010) have derived general expressions for the spherical field components of an axisymmetric multipole (m = 0 and 1 respectively described in figure 3.1) of arbitrary degree ℓ:

Some of the stellar magnetic fields characteristics such as its polar order and axisymmetry can be simply described using the multipole number ℓ and axis-symmetry number m. However we are assuming perfect axisymmetry to model the stellar magnetic fields, that means the magnetic field $\mathbf{B} = (B_r, B_\theta, 0)$ in spherical polar coordinates. We assume the magnetic moments are aligned with the stekkar rotation axis, which is also aligned with the stellar rotation axis (z-axis). Perfect axisymetry would not be present in real star's, Figure 2.1 would be an example of this. The convective zone of the stellar interior that generates the magnetic field would have inconsistent movement causing the magnetic field to be just as inconsistent, we must also consider the azimuthal dependence on the shape of the field that would make the problem 3 dimensional an much more complicated. And so assuming axisymmetry allows progress to be made semi-analytically.

These mentioned ℓ numbers can be visually represented in figure 3.1. Almost all published magnetic maps of fully convective and partially convective PMS star's with small radiative cores have a combination of dipole and octupole fields (dominant $(\ell = 1, m = 0)$ and $(\ell = 3, m = 0)$ field modes (Gregory et al. 2014)). The magnetic maps published were used to create a magnetic HR diagram as shown in Figure 2.5. A PMS star's location in the HR diagram determines its internal structure and the global properties of its large-scale magnetic field. Once we have established the field configuration of the star we want to model we can determine the shape of the star's magnetic field, allowing us to then find the maximum sized field lines that can hold

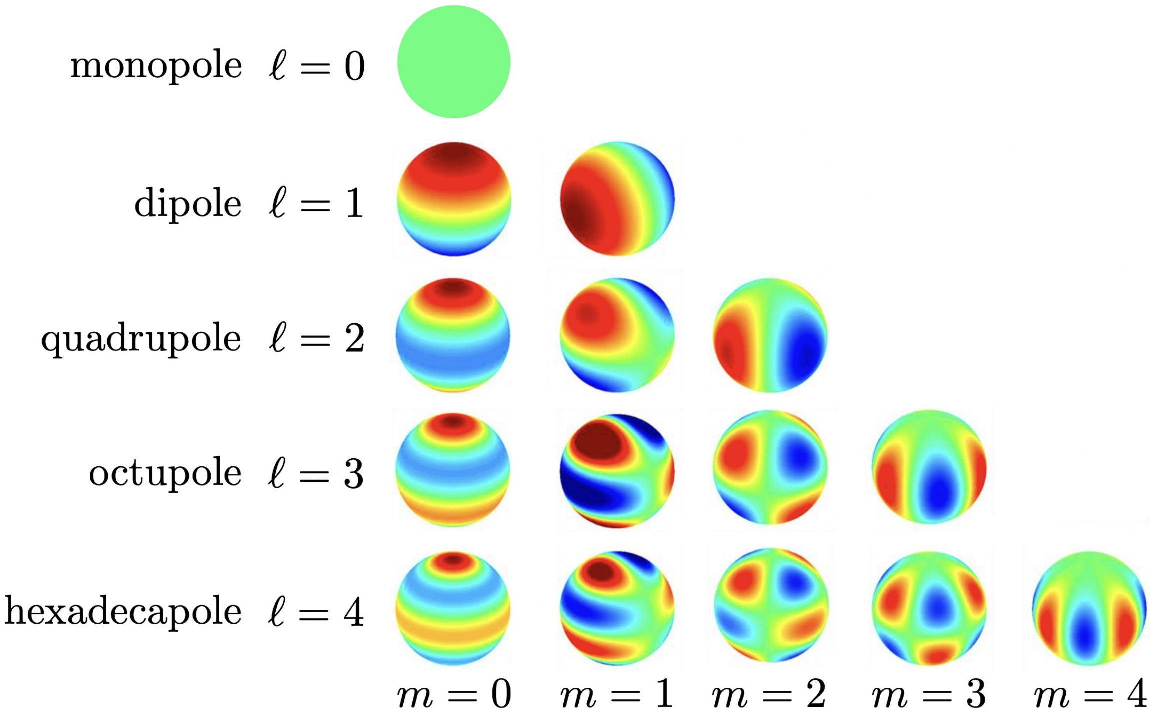

Figure 3.1: Spherical harmonics to show the surface distribution of magnetic field across the stellar surface. Multipole number ℓ and order number m are not limited as shown in the figure. Colored regions represent the polarity of the magnetic field at that point with blue and red being opposite in polarity from one another (blue/red denoting negative/positive respectively). Every other color acts as a gradient to show change in polarity around the star's surface. Field lines can be drawn connecting the regions of opposite polarity producing stellar magnetic field maps as shown in figure 2.1. figure from MA41006 lecture notes

the X-ray emitting plasma.

In order to determine the emission measure in equation 6 we need to integrate over the enclosed X-ray emitting volume V as shown in equation 7 which depends mainly on the dimensionless parameter ξ and gas pressure 17 which happens to also depend on the dimensionless parameter ξ, thetal position θ and ratio B_θ/B_r as seen below:

$$B_r = B_*^{\ell,pole}\left(\frac{1}{\xi}\right)^{\ell+2} P_\ell(cos\theta), \tag{18}$$

$$B_\theta = \frac{B_*^{\ell,pole}}{\ell+1}\left(\frac{1}{\xi}\right)^{\ell+2} P_{\ell 1}(cos\theta), \tag{19}$$

$P_l(cos\theta)$ and $P_{l1}(cos\theta)$ are the Legendre polynomials and associated legendre functions respectfully of order ℓ and m. This allows us to fully determine the gas pressure in equation 17 at some point along a magnetic field line loop as well as model the star's magnetic field and create simplified 2 dimensional models of what is shown in figure 2.1.

As discussed in section §2.2 the X-ray emitting volume is defined by the trapped volume under the stellar corona. Güdel (2009) thought the maximum radius at which the stellar magnetic field can contain the hot coronal plasma could be found. There is a point at which the gas pressure equation 17, from the plasma along the field lines will exceed the star's magnetic pressure equation 20. At this point the plasma would be ripped away from the star's field lines leaving only the more compact field lines which are what becomes the star's corona (Güdel 2009). I used this information in my models when determining what would be considered part of the X-ray emitting volume. The magnetic pressure from the star exerted onto the corona can be written mathematically as (Garren & Chen 1994):

$$P_B = \frac{B^2}{8\pi} \quad \text{where,} \quad B^2 = B_\theta^2 + B_r^2 \tag{20}$$

The next step would be to model the star's magnetic field as a guide to find where the maximum radius at which the field can hold the hot coronal plasma which in turn would give us the enclosed X-ray emitting volume represented by the integral in equation 7. Modelling the star's magnetic field would involve picking an arbitrary point at distance r from the star's surface, measuring the field strength at that point using equation 19. Then knowing the field strength at this arbitrary point we can trace the field line that passes through this point that we know has identical magnitude to the starting point but changing B_θ/B_r ratio. Tracing the field line would involve calculating the change in θ and r using how B_θ or B_r changes with the magnitude of B. The shape of the field line is described by the differential equations,

$$\frac{B_r}{dr} = \frac{B_\theta}{rd\theta} = \frac{\mathbf{B}}{ds} \tag{21}$$

where ds is some small element of length measured along the path of a magnetic loop. By numerically solving the differential equations for a specific magnetic field geometry (from equations 19, we can trace the shape of the field line loops. in turn we can then calculate the gas and magnetic pressures at each point along the magnetic field line.

At each point in the field line we would calculate the ratio of magnetic to gas pressure, equations 20 and 17 and if the gas pressure doesn't exceed the magnetic pressure anywhere along that field line we then move our arbitrary starting point out with increasing distance from the surface of the star until it does for greater sized field lines. At any point along the field line where the gas pressure is equal to or less than the magnetic pressure would be considered the stellar corona (Güdel 2009) and we can evaluate the pressure at the foot points of the corona ($P_0 = KB_0^2$)

and the volume integral in equation 7 then ultimately the X-ray luminosity in equation 1.

3.2 Axisymetric Models

The following plots are 2-Dimensional models of ℓ'th order field topology's that make up the the majority of my project work. This is to firstly prove that the X-ray emitting volume under the stellar corona decreases with complexity (increasing ℓ) and in turn to prove decreasing X-ray luminosity with complexity (since X-ray luminosity is proportional to the enclosed volume equation 1). ℓ could also represent the number of shells of closed field lines as you move from the north to south pole of the star in the following models.

$\log K$	$R_*/R_\odot$	$M_*/M_\odot$	$B_*^{\ell,pole}(G)$	$P_{rot}(d)$	$\log T(K)$
-5	2	0.5	1000	5	7

Table 3.1: Parameters used for all ℓ'th number multipole models below to allow fair comparison in results. These are typiical PMS star parameters

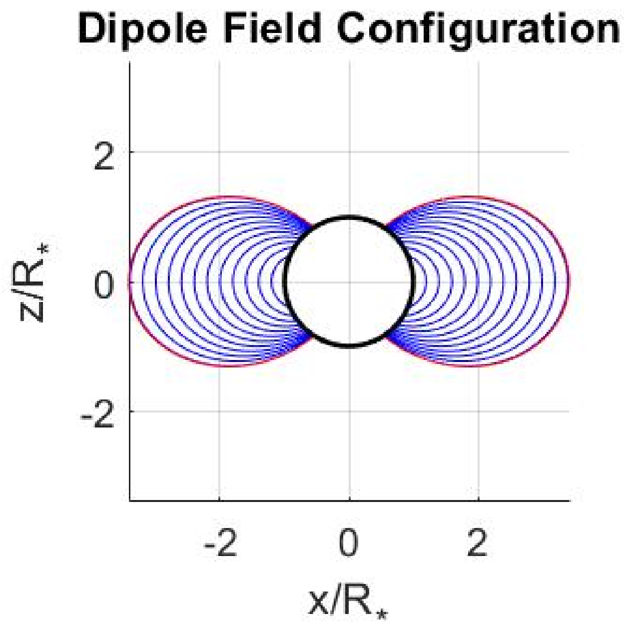

Figure 3.2: Figure Shows 2-D model of a dipole field topology ($\ell = 1$), where the black circular object in the center represents the star. The Blue lines represent the magnetic field lines of the stellar corona and the red lines represent the maximum sized field line that can hold the X-ray emitting plasma. Field lines that extend beyond the red line are pulled open by the gas pressure exceeding the magnetic pressure.

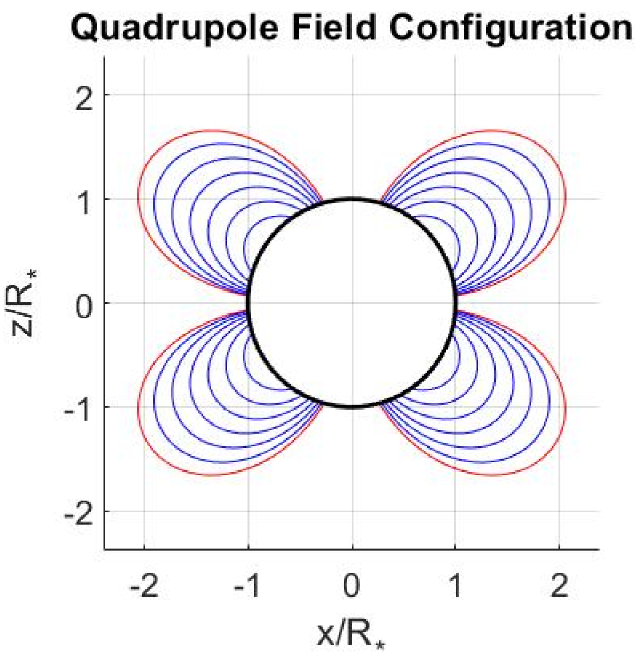

Figure 3.3: Figure Shows 2-D model of a quadrupole field topology ($\ell = 2$)

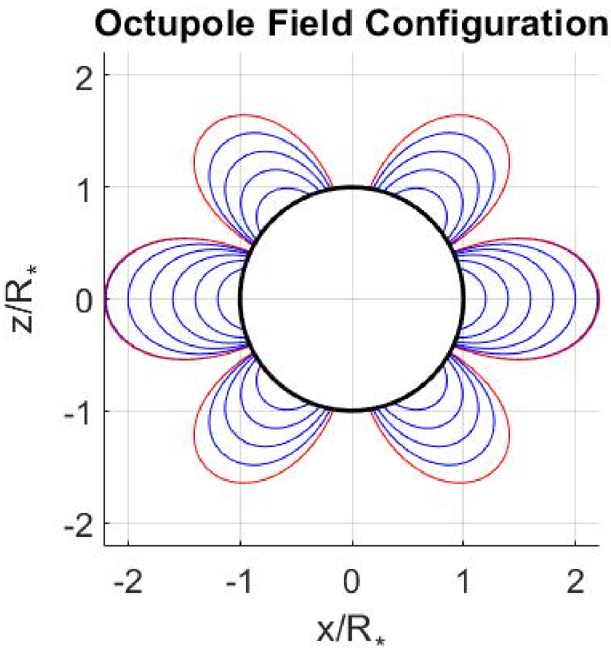

Figure 3.4: Figure Shows 2-D model of an octupole field topology ($\ell = 3$)

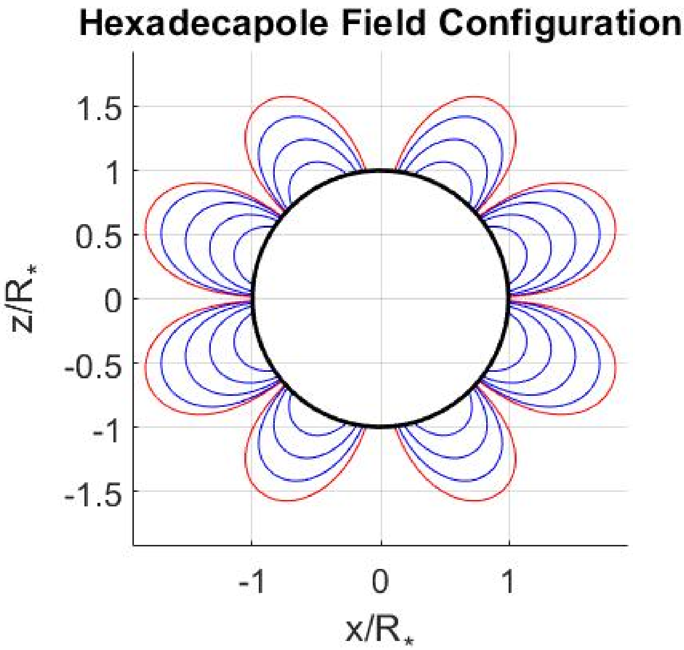

Figure 3.5: Figure Shows 2-D model of an hexadecapole field topology ($\ell = 4$)

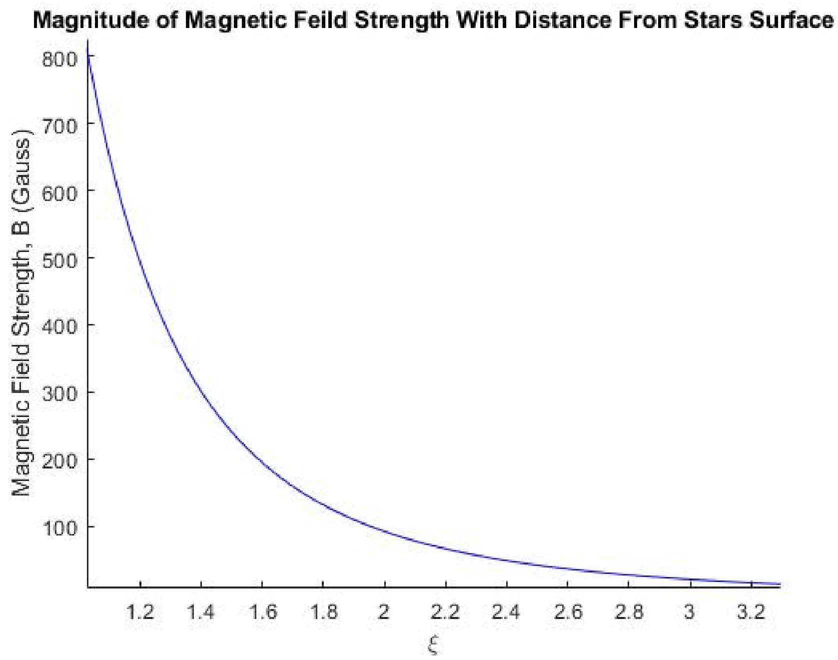

Figure 3.6: Figure shows star's magnetic field influence (B_*) as distance from the stellar surface increases (ξ) for a dipole field configuration, along the red magnetic field loop sketched in Figure 3.2.

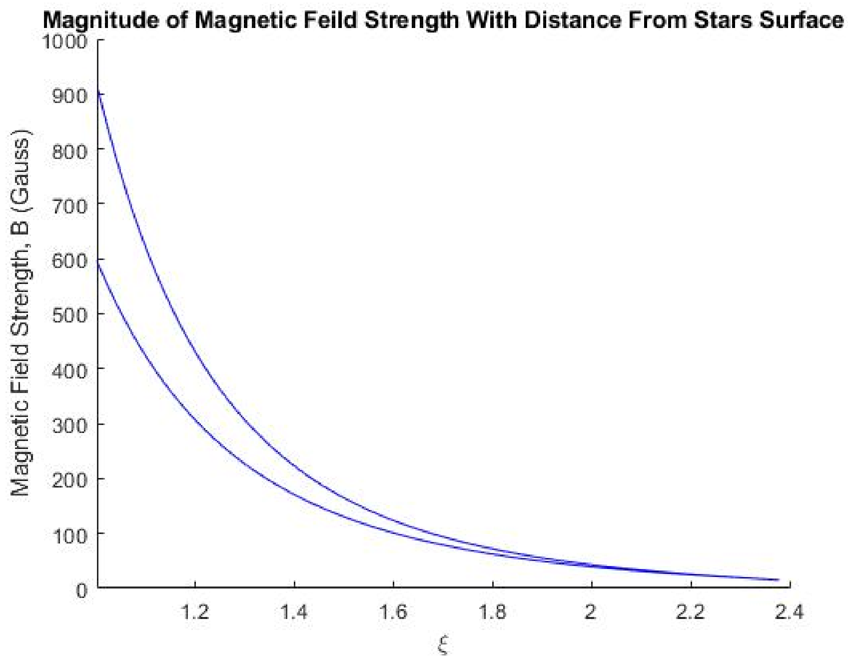

Figure 3.7: Figure shows star's magnetic field influence (B_*) as distance from the stellar surface increases (ξ) for a quadrupole field configuration, along the red magnetic field loop sketched in Figure 3.3.

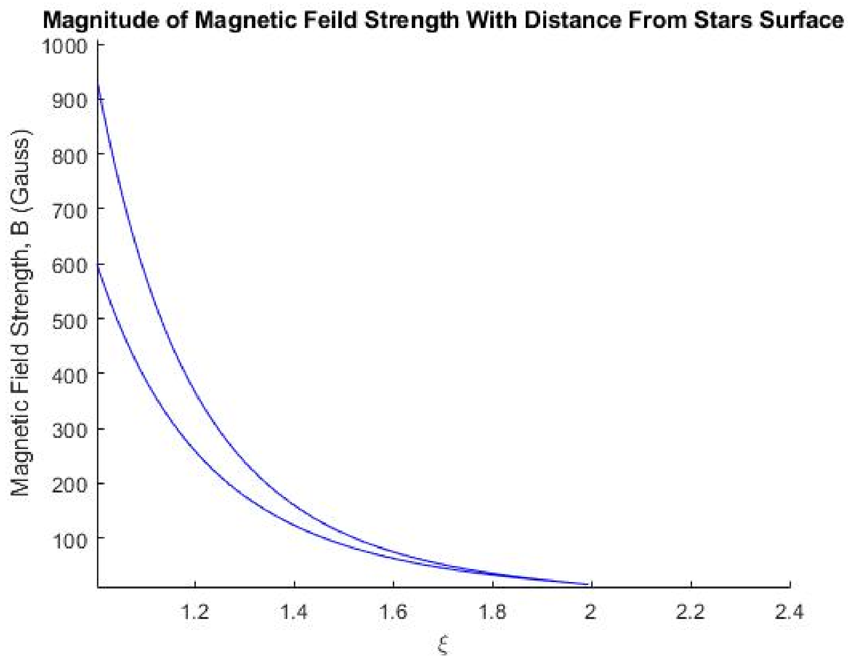

Figure 3.8: Figure shows star's magnetic field influence (B_*) as distance from the stellar surface increases (ξ) for an octupole field configuration, along the red magnetic field loop sketched in Figure 3.4.

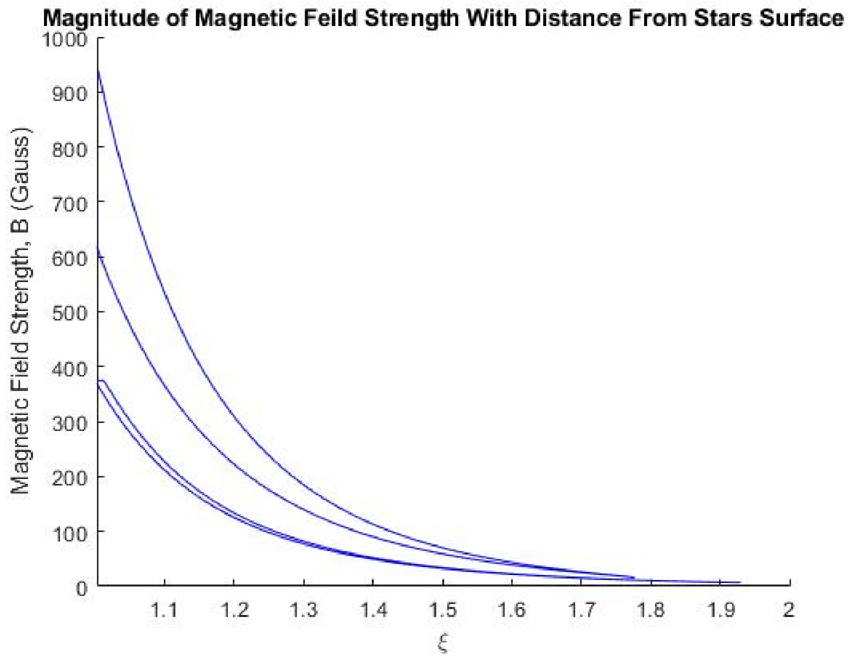

Figure 3.9: Figure shows star's magnetic field influence (B_*) as distance from the stellar surface increases (ξ) for a hexadecapole field configuration, along the red magnetic field loop sketched in Figure 3.5.

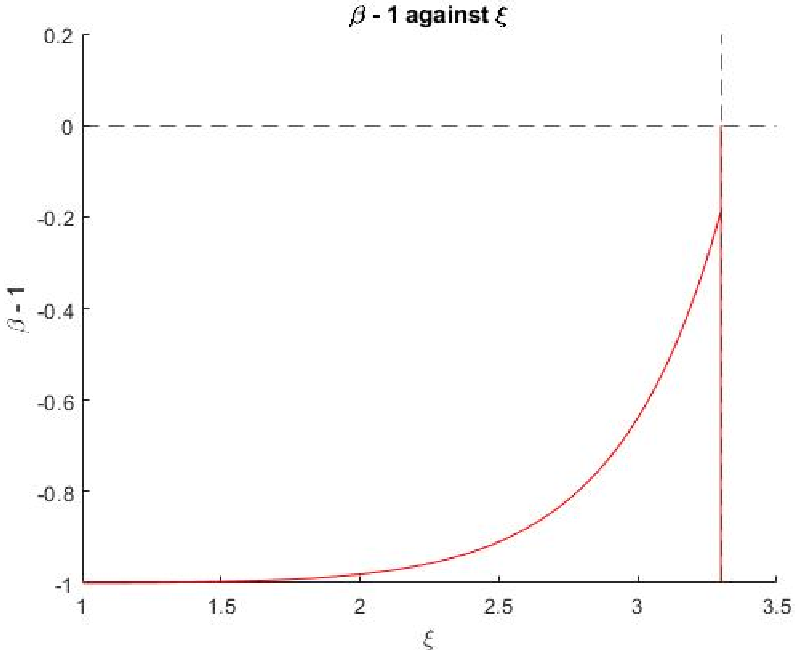

Figure 3.10: Figure shows magnetic pressure to gas pressure ratio function where, $\beta = p_{gas}/p_{mag}$ r_{max} occurs when $p_{gas}/p_{mag} = 1$. And so interception with x-axis ($\beta - 1 = 0$) indicates the max radial extent of corona corresponding to the dipole field configuration in Figure 3.2

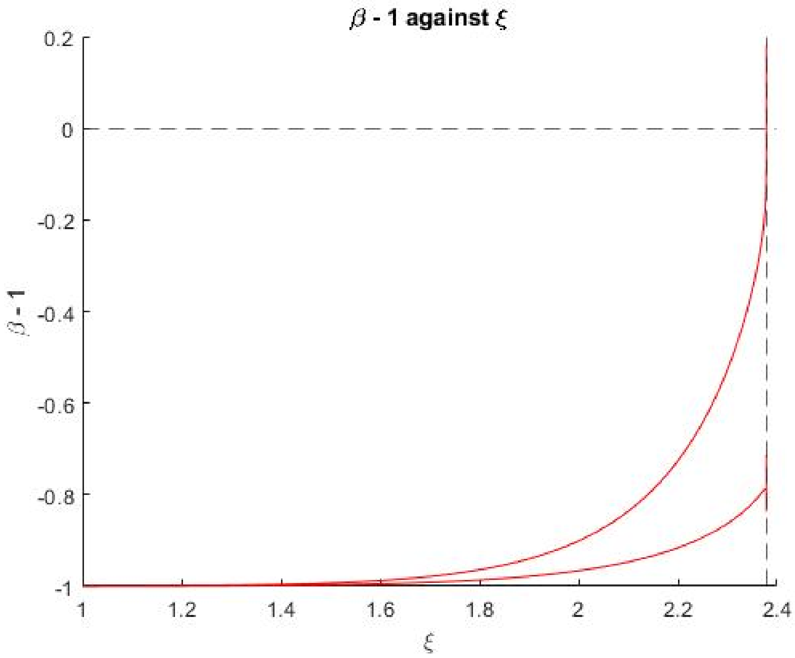

Figure 3.11: Figure shows magnetic pressure to gas pressure ratio function where, $\beta = p_{gas}/p_{mag}$ r_{max} occurs when $p_{gas}/p_{mag} = 1$. And so interception with x-axis ($\beta - 1 = 0$) indicates the max radial extent of corona corresponding to the Quadrupole field configuration in Figure 3.3.

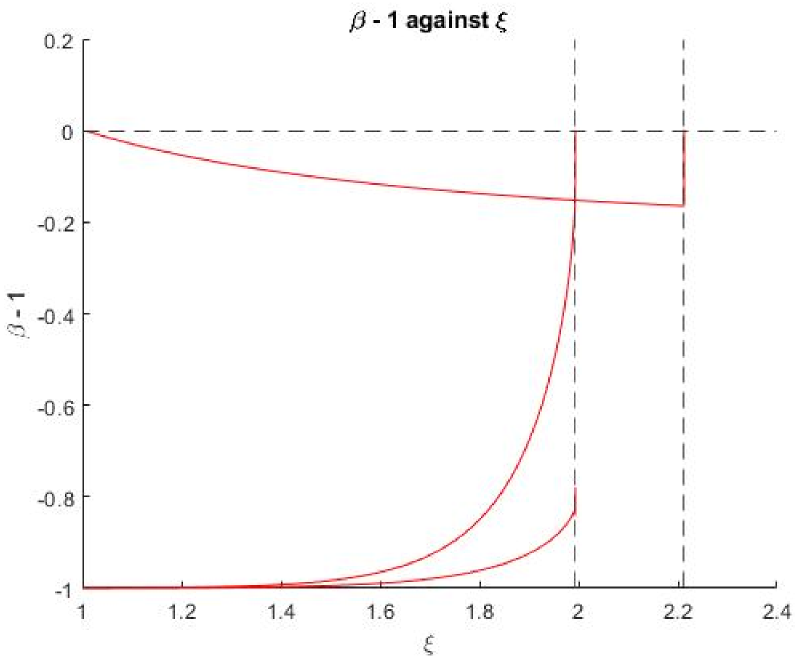

Figure 3.12: Figure shows magnetic pressure to gas pressure ratio function where, $\beta = p_{gas}/p_{mag}$ r_{max} occurs when $p_{gas}/p_{mag} = 1$. And so interception with x-axis ($\beta - 1 = 0$) indicates the max radial extent of corona corresponding to the Octupole field configuration in Figure 3.4. The multiple r_{max} values given show the extent of each shell present in a quadrant of Figure 3.4.

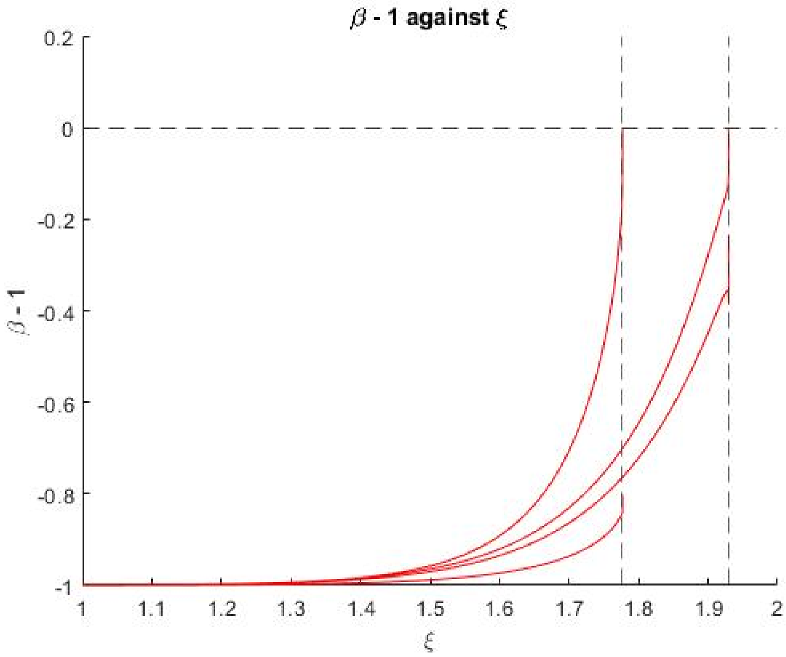

Figure 3.13: Figure shows magnetic pressure to gas pressure ratio function where, $\beta = p_{gas}/p_{mag}$ r_{max} occurs when $p_{gas}/p_{mag} = 1$. And so interception with x-axis ($\beta - 1 = 0$) indicates the max radial extent of corona corresponding to the Hexadecapolefield configuration in Figure 3.5. The multiple r_{max} values given show the extent of each shell present in a quadrant of Figure 3.5.

Where β is the ratio of gas pressure to magnetic pressure (P/P_B) at radial distance r from the star's surface (or ξ). Subtracting 1 from β creates a root to the function equal to 0, then the root occurs when $P = P_B$ corresponding to the maximum distance (ξ) the field lines can hold the X-ray emitting plasma (r_{max}).

Once we have modelled the magnetic fields of given ℓ numbers we can numerically calculate the enclosed area under r_{max} and therefore the enclosed volume as the magnetic fields are rotationally symmetric about the z-axis ($d\phi = 0$) and then use this to calculate the emission measure, equation 6. The r_{max}'s and calculated volumes for each model above are found in Table 3.2 below.

ℓ	coronal extent r_{max}	volume, V	ε_M
1	3.4209	73.35	3126.78
2	2.3781	12.88	738.88
3	1.993 2.2121	15.50	316.07
4	1.7764 1.9295	7.25	147.62

Table 3.2: Calculated r_{max}'s, volumes and emission measures ε_M for given magnetic field topology's (ℓ). r_{max} and volume have dimensionless units since they are relative to the radius of the star e.g. $r_{max} = 3$ extends to 3 times the radius of the star ect.

The above magnetic field models (Figures 3.2, 3.3, 3.4 and 3.5) demonstrate an increase in magnetic field complexity with field order ℓ, the change in magnetic field strength with distance from the stellar surface and the maximum radial field distance from the stellar surface at which the X-ray emitting plasma can be held (red line in configuration plot or route of function). The plots show what happens to the X-ray emitting volume when the field becomes more complex (as the ℓ number increases), we can see that increasing the field complexity increases the number of shells around the star which would appear to increase the X-ray emitting volume however this is not the case. Table 3.2 shows both a decrease in the maximum radial extent and volume with an increase in field complexity with the exception of $\ell = 3$ that shows a higher volume that $\ell = 2$ but lower emission measure (ε_M), I believe this to be a problem in my code. The decrease in maximum radial extent r_{max} has more effect on the overall X-ray emitting volume than the increase in the number of shells around the star, This is because it is easier for the stellar wind to pull open the larger field lines because of the weaker field strength at larger distances from the star as demonstrated in the field strength plots above that follow the relationship $B = |\hat{B}| \propto \frac{1}{r^{\ell+2}}$, where the field strength drops faster with radius for larger ℓ numbers.

$$V_{dipole} = \frac{4\pi}{3} r_{max}^3 \frac{2}{35} \left(1 - \frac{1}{r_{max}}\right)^{1.5} \left(8 + \frac{12}{r_{max}} + \frac{15}{r_{max}^2}\right) \tag{22}$$

Equation 22 above shows the analytical expression for the volume contained within a dipole loop. Using this equation and the same r_{max} given in Table 3.2 for $\ell = 1$, we get a volume of 73.57 cubed units. When calculating this volume numerically in my code i used a numerical grid and evaluated all the grid points contained within the loop in question. Comparing this value to the numerical value given in 3.2 (73.93) we can estimate the accuracy of the numerical calculation in my code (rounded to ± 0.40 cubed units) and assume the same level of accuracy for a subsequent volume calculation (different ℓ numbers).

4 Dipole-Octupole magnetic fields

As discussed previously it is possible for a star's field complexity to evolve to a point where two ore more ℓ'th order pole configurations can be present. Table 4.2 shows 3 star's with dipole-octupole fields and their observational and derived parameters. The following models are used to test the decreasing X-ray luminosity with field complexity further, they also compare different field strength combinations of B_{oct}/B_{dip} and test their effects on the field complexity and 'null point' discussed later on. For combination multipoles like in Table 4.2, calculating the field strength components would be as simple as adding the field strengths (equation 19) of each ℓ'th order magneitc field component, where $\ell = 1$ for the dipole component and $\ell = 3$ for the octupole:

$$B_r = B_{dip}\left(\frac{1}{\xi}\right)^3 P_{1,0}(cos\theta) + B_{oct}^3\left(\frac{1}{\xi}\right)^5 P_{3,0}(cos\theta), \tag{23}$$

$$B_\theta = \frac{B_{dip}}{2}\left(\frac{1}{\xi}\right)^3 P_{1,1}(cos\theta) + \frac{B_{oct}^3}{4}\left(\frac{1}{\xi}\right)^5 P_{3,1}(cos\theta) \tag{24}$$

Star	$\log K$	$R_*/R_\odot$	$M_*/M_\odot$	$B_{dip}(G)$	$B_{oct}(G)$	$P_{rot}(d)$	$\log T_X(K)$
AA Tau	-6.7	2.00	0.70	1720	500	8.20	7.43
BP Tau	-6.9	1.95	0.70	1220	1600	7.60	7.06
V2129 Oph	-6.9	2.00	1.35	740	280	6.53	7.05

Table 4.1: Table showing 3 dipole + octupole star's with accompanying proportionality constant K, stellar radius R_*, stellar mass M_*, magnetic field strength of both the dipole component B_{dip} and the octupole component B_{oct}, the stellar rotation period P_{rot} and the coronal temperature T_X, data from (Johnstone et al. 2014).

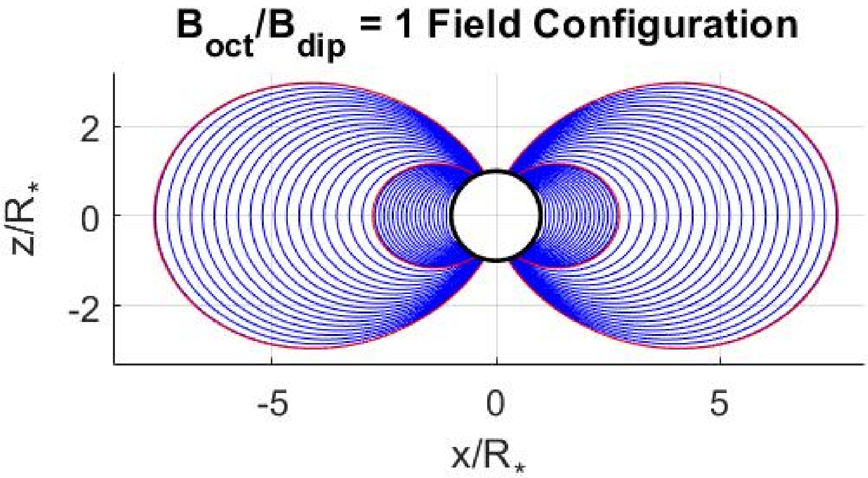

Figure 4.1: Figure Shows 2-D model of an dipole-octupole combination field topology ($\ell = 1, \ell = 3$), with a B_{oct}/B_{dip} ratio equal to 1. Where the smaller area enclosed by the red line can be ignored as an anomaly.

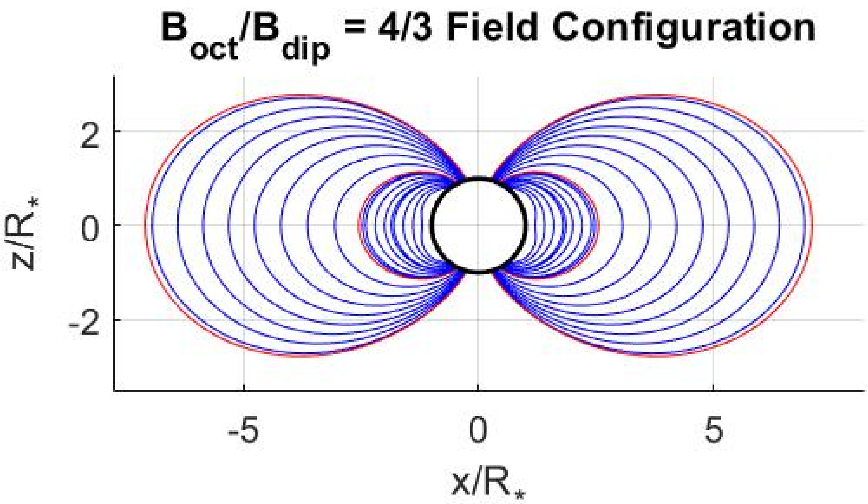

Figure 4.2: Figure Shows 2-D model of an dipole-octupole combination field topology ($\ell = 1, \ell = 3$), with a B_{oct}/B_{dip} ratio equal to 4/3.

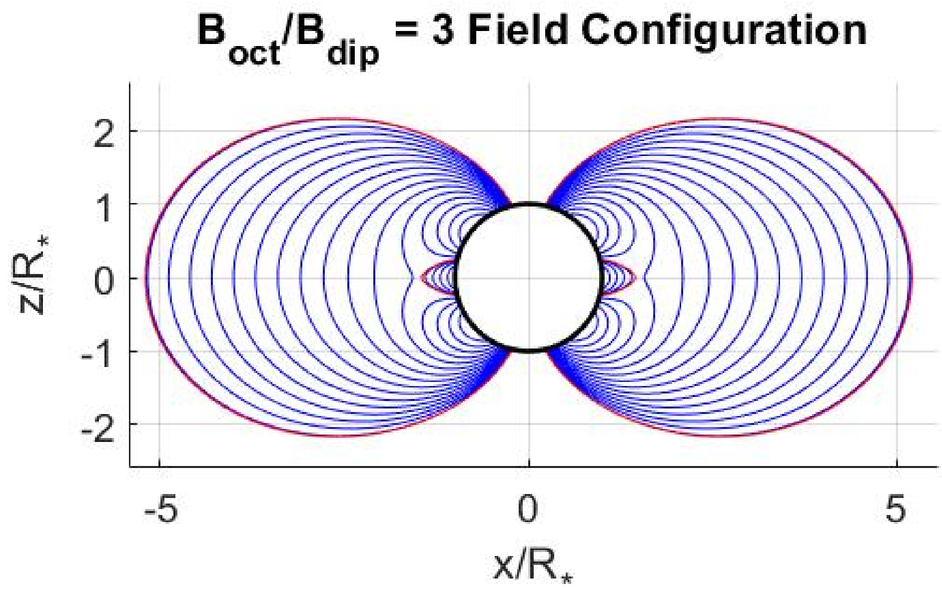

Figure 4.3: Figure Shows 2-D model of an dipole-octupole combination field topology ($\ell = 1, \ell = 3$), with a B_{oct}/B_{dip} ratio equal to 3.

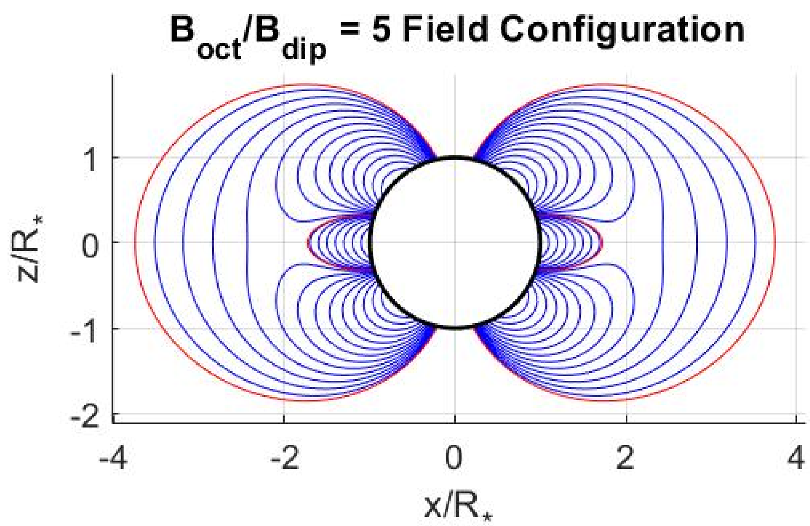

Figure 4.4: Figure Shows 2-D model of an dipole-octupole combination field topology ($\ell = 1, \ell = 3$), with a B_{oct}/B_{dip} ratio equal to 5.

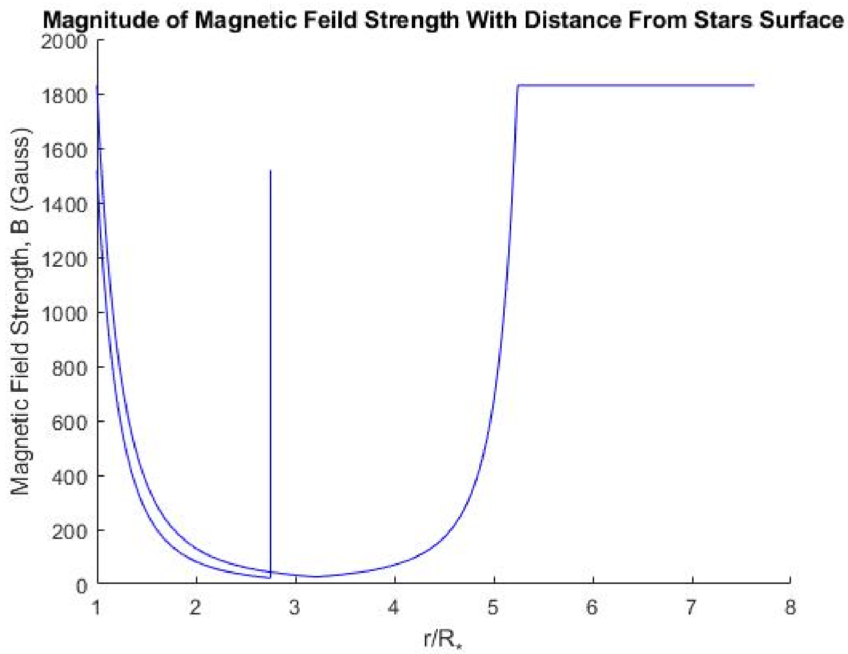

Figure 4.5: dipole-octupole ($\ell = 1, \ell = 3$) field strength with distance from stellar surface along the red line in figure 4.1, B_{oct}/B_{dip} ratio equal to 1.

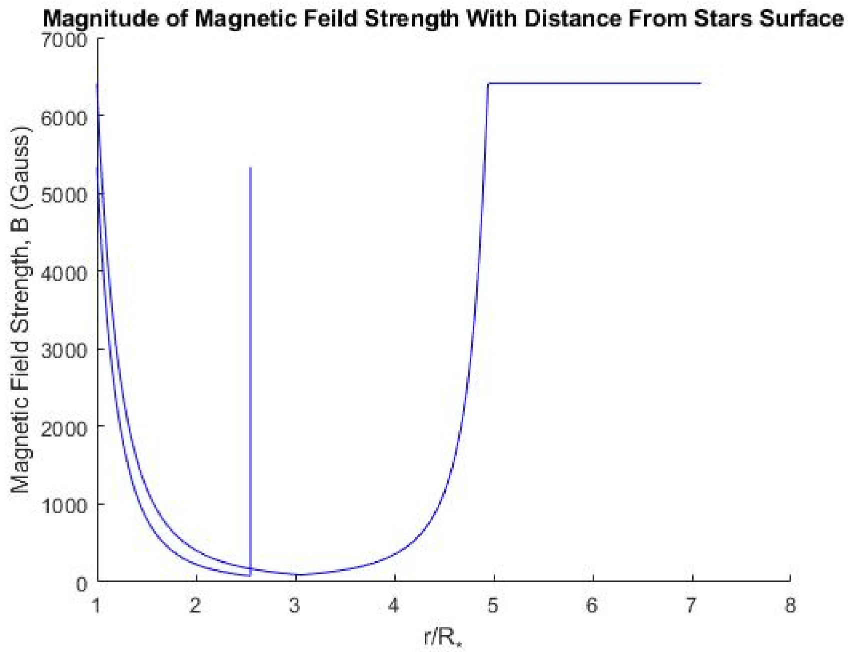

Figure 4.6: dipole-octupole ($\ell = 1, \ell = 3$) field strength with distance from stellar surface along the red line in figure 4.2, B_{oct}/B_{dip} ratio equal to 4/3.

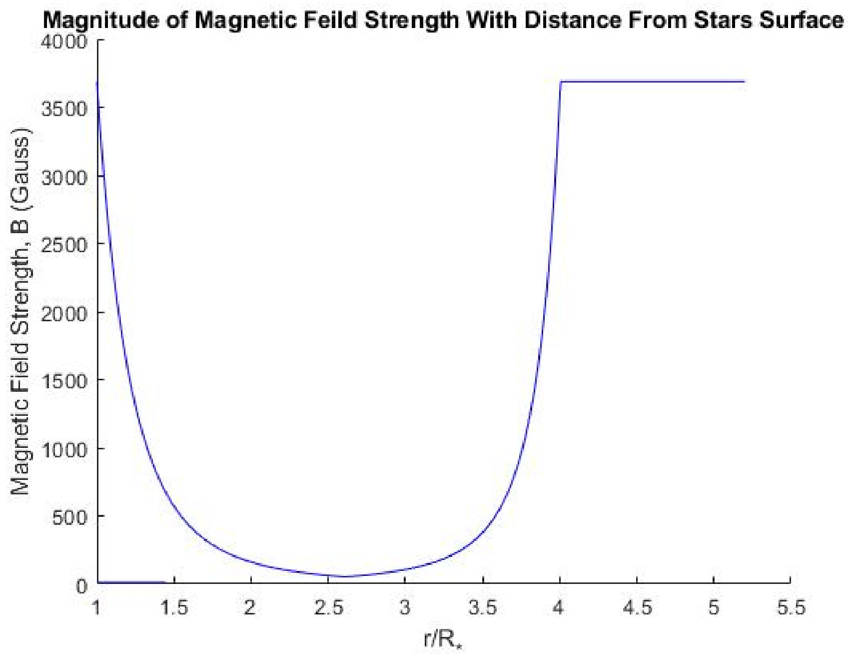

Figure 4.7: dipole-octupole ($\ell = 1, \ell = 3$) field strength with distance from stellar surface along the red line in figure 4.3, B_{oct}/B_{dip} ratio equal to 3.

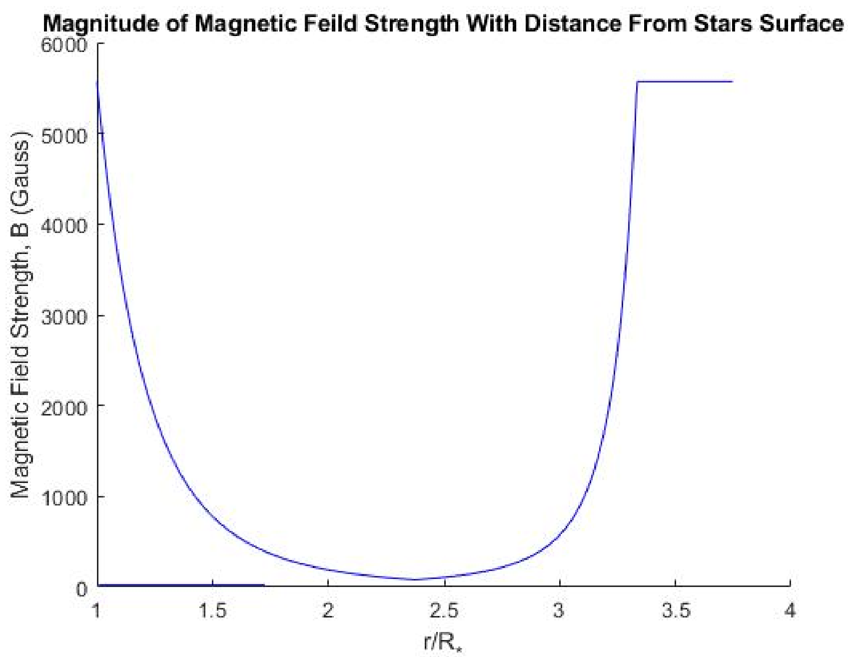

Figure 4.8: dipole-octupole ($\ell = 1, \ell = 3$) field strength with distance from stellar surface along the red line in figure 4.4, B_{oct}/B_{dip} ratio equal to 5.

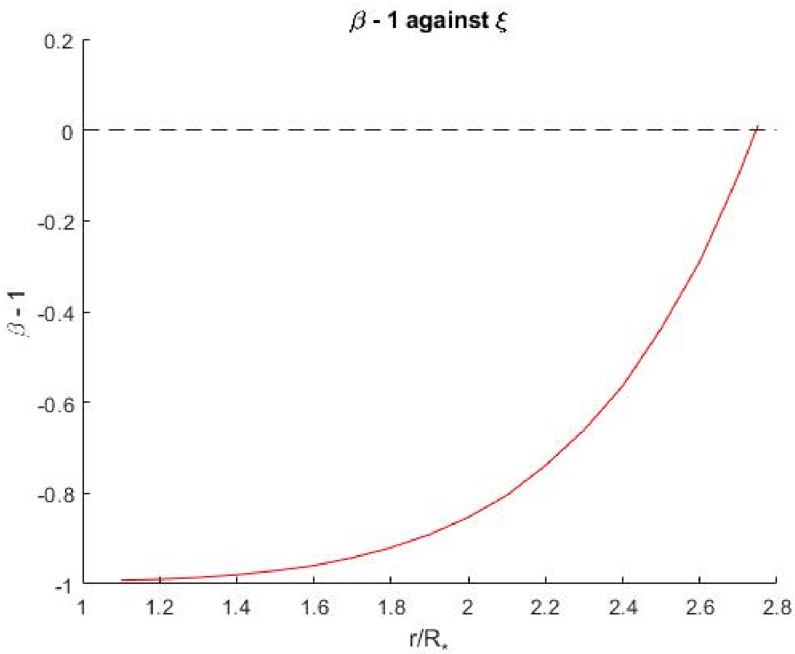

Figure 4.9: dipole-octupole ($\ell = 1, \ell = 3$) function showing the maximum radial field extent that the X-ray emitting plasma can be held for B_{oct}/B_{dip} ratio equal to 1. Multiple roots correspond to the different values of r_{max} seen in corresponding model, Figure 4.1.

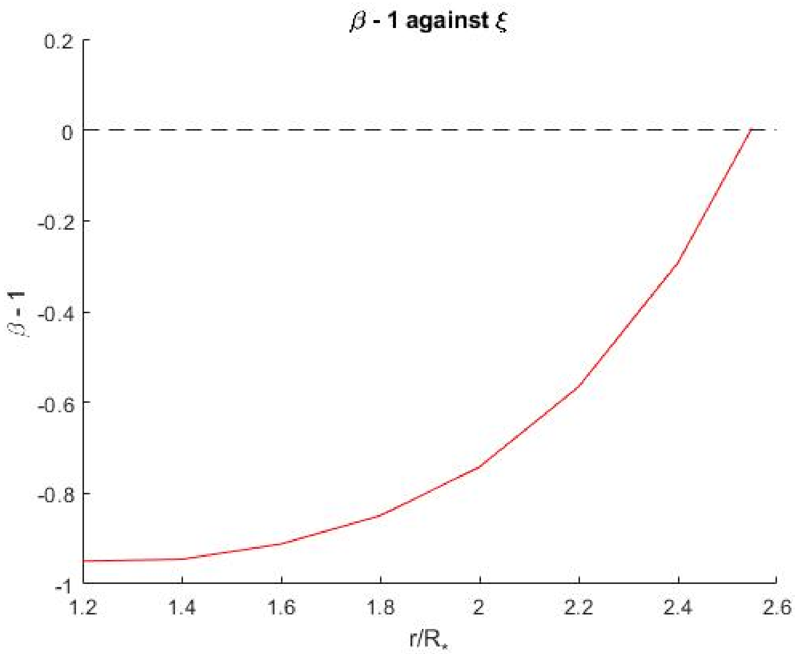

Figure 4.10: dipole-octupole ($\ell = 1, \ell = 3$) function showing the maximum radial field extent that the X-ray emitting plasma can be held for B_{oct}/B_{dip} ratio equal to 4/3. Corresponds to Figure 4.2.

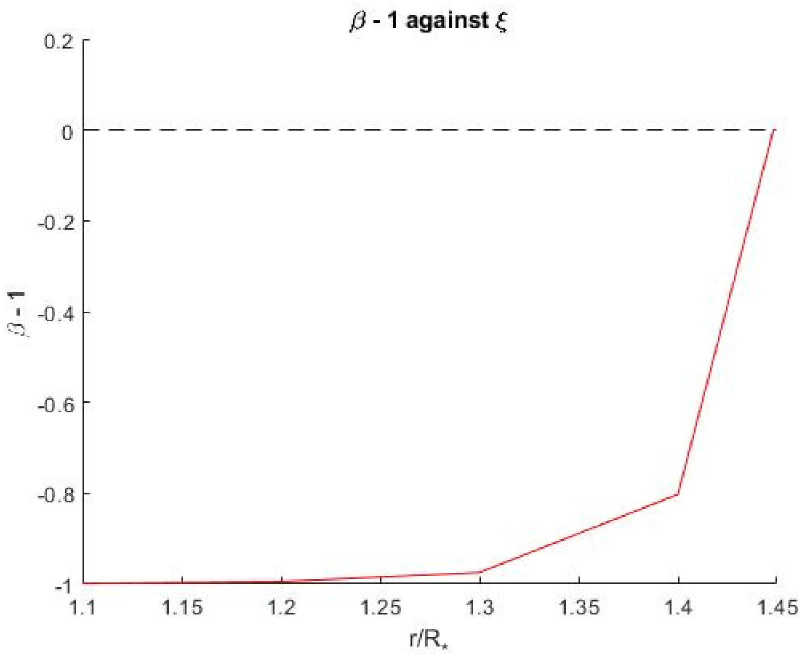

Figure 4.11: dipole-octupole ($\ell = 1, \ell = 3$) function showing the maximum radial field extent that the X-ray emitting plasma can be held for B_{oct}/B_{dip} ratio equal to 3. Corresponds to Figure 4.3.

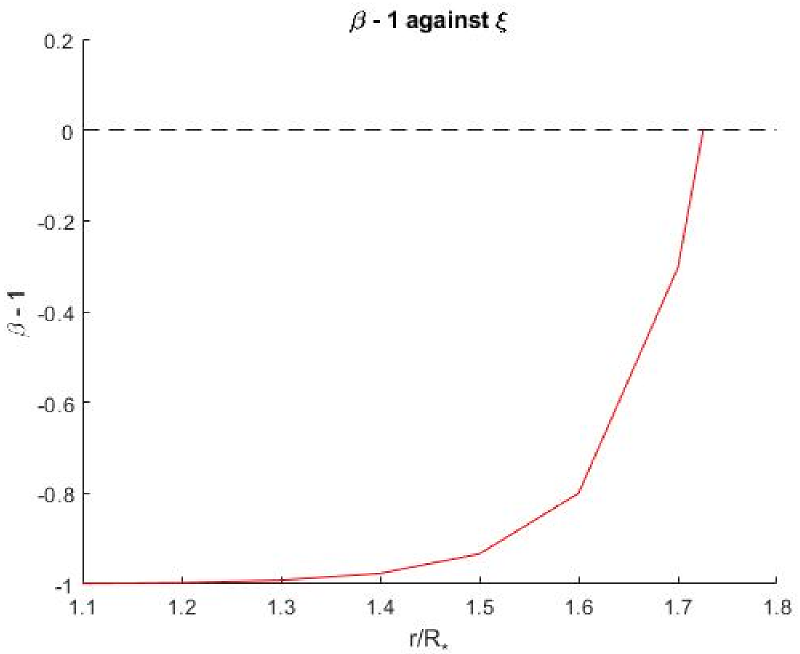

Figure 4.12: dipole-octupole ($\ell = 1, \ell = 3$) function showing the maximum radial field extent that the X-ray emitting plasma can be held for B_{oct}/B_{dip} ratio equal to 5. Corresponds to Figure 4.4.

$\log K$	$R_*/R_\odot$	$M_*/M_\odot$	$P_{rot}(d)$	$\log T(K)$
-5	2	0.5	5	7

Table 4.2: Parameters used for all combination ℓ'th number multipole models to allow fair comparison in results.

B_{oct}/B_{dip}	coronal extent r_{max}		volume, V	ε_M
1	3.2105	2.7508	248.05	102858.98
4/3	3.0576	2.5492	333.3477	21241574.87
3	2.6093	1.4483	22.85	85077.50
5	2.373	1.7258	20.63	392113.02

Table 4.3: Calculated r_{max}'s, volumes and emission measures ε_M for given magnetic field topology's (ℓ). r_{max} and volume have dimensionless units since they are relative to the radius of the star e.g. $r_{max} = 3$ extends to 3 times the radius of the star etc.

The above stellar magnetic models differ a lot from the previous models with changing ℓ numbers since they have fixed ℓ numbers ($\ell = 1$, $\ell = 3$) that describe a dipole-octupole combination field configuration. We change how much which field component dominates the other for example a B_{oct}/B_{dip} ratio equal to 5 would mean the field strength of the octupole component would be 5 times the magnitude of the dipole component. Dipole-octupole combination field configurations do exist in star's however real models would be much more complex (many more factors to consider, non-uniform stellar interior, non-axisymetric ect.) as discussed in section §2.1. As seen from my results regarding the X-ray emitting volume under the dipole-octupole field configuration in Table 4.3, they are not what i would expect to see for a increasing field complexity (in this case an increase in B_{oct}/B_{dip}) and therefore do not support the speculated decay of X-ray emission with increase in field complexity. However i am confidant these results are due to problems in my code and are not proper results that would argue against the speculation and the rest of the analytical work done in my project. Therefore i would regard my dipole-octupole results as tentative, with more work required to fully test the code.

The problem with the analytics in my code would be due to the existence of the null-point in dipole-octupole field configurations, which is a point in the star's magnetic field where the magnitude of the field strength at that point would be equal to 0 where the dipole and octupole field components cancel each other completely. Gregory & Donati (2011) describe the null point in more detail. My code would recognise that the gas pressure would always exceed the magnetic pressure at this point and label it as a smaller enclosed X-ray emitting volume an add it to the total X-ray emitting volume the dipole-octupole configuration models above show this smaller volume as the smaller area enclosed by the red line (explaining the existence of two r_{max}'s in Table 4.3). This ultimately calculated a larger X-ray emitting volume than intended an in turn a larger X-ray luminosity (X-ray luminosity results section §**??**) and so does not support the main aim of my project.

In between the smaller r_{max}'s in Table 4.3 and the next closed field line in the above dipole-octupole field configuration models would host the null-point, you can also see from the models that as we increase the B_{oct}/B_{dip} ratio the null point becomes more visible and exterior to the star. Figure 4.2 shows a model where the null point is at the surface of the star indicated by the small area without field lines on the star's surface. Any B_{oct}/B_{dip} ratios below a value of 4/3 (Figure 4.1 where smaller r_{max} can be ignored, I cannot explain its presence) would host the null point within the star's interior, while B_{oct}/B_{dip} ratios higher than 4/3 would have a null point exterior to the star (Donati et al. 2011). Gregory et al. (2016) provides the null points position relative to the star with the following relationship:

$$\frac{r_{null}}{R_*} = \left(\frac{3}{4}\frac{B_{oct}}{B_{dip}}\right)^{\frac{1}{2}} \tag{25}$$

B_{oct}/B_{dip}	model's r_{max}	calculated r_{max}
1	2.7508	0.8660
4/3	2.5492	1.0000
3	1.4483	1.5000
5	1.7258	1.9365

Table 4.4: r_{max} of B_{oct}/B_{dip} models in Table 4.3 compared to calculated r_{max}'s using equation .

Table 4.4 shows how my modeled values of r_{max} compare to calculated values using equation , the first two modeled values can be ignored since i believe them to be a problem in the code. Calculated values of r_{max} for B_{oct}/B_{dip} equal to 3 and 5 seem to be somewhat consistent with whats expected, which was that the null point would be in between the smaller area bordered by the red line and the next closed field line out from the star. Figure 4.3 shows a great example of the null point seen by the connected field line that's closest to the star and where the modeled value of r_{max} is not that much smaller than the calculated value. I think the presence of the null point wouldn't affect the enclosed X-ray emitting volume much, I speculate that any X-ray emitting plasma that would find itself near the null point would form along the stronger field lines around the null point, the configuration models show that the gas pressure exceeds the star's magnetic field at radii larger than the radius of the null point which is what makes me speculate this.

5 X-ray Luminosities

The following section shows the relationships between the X-ray emitting volume and calculated X-ray luminosity's with an increase in magnetic field complexity (increasing ℓ and B_{oct}/B_{dip} ratio). Using our results in Table's 3.2 and 4.3 we can graph an increasing field complexity with; the maximum coronal extent r_{max} shown in Figures 5.1 and 5.4, the enclosed X-ray emitting volume (numerically calculated in code) shown in Figures 5.2 and 5.5, and the calculated X-ray luminosity shown in Figures 5.3 and 5.6.

ℓ	L_X, $ergs^{-1}$
1	1.27e+32
2	3.00e+31
3	1.28e+31
4	5.99e+30

Table 5.1: Table showing numerically evaluated X-ray luminosity's (L_X) of magnetic field topology models for given ℓ numbers; $\ell = 1$, $\ell = 2$, $\ell = 3$ and $\ell = 4$ corresponding to Figures; 3.2, 3.3, 3.4 and 3.5 respectively.

B_{oct}/B_{dip}	L_X, $ergs^{-1}$
1	4.17e+33
4/3	8.62e+35
3	3.45e+33
5	1.60e+34

Table 5.2: Table showing numerically evaluated X-ray luminosity's (L_X) of a dipole + octupole magnetic field topology model for given B_{oct}/B_{dip} ratios; $B_{oct}/B_{dip} = 1$, $B_{oct}/B_{dip} = 4/3$, $B_{oct}/B_{dip} = 3$ and $B_{oct}/B_{dip} = 5$ corresponding to Figures; 4.1, 4.2, 4.3 and 4.4 respectively.

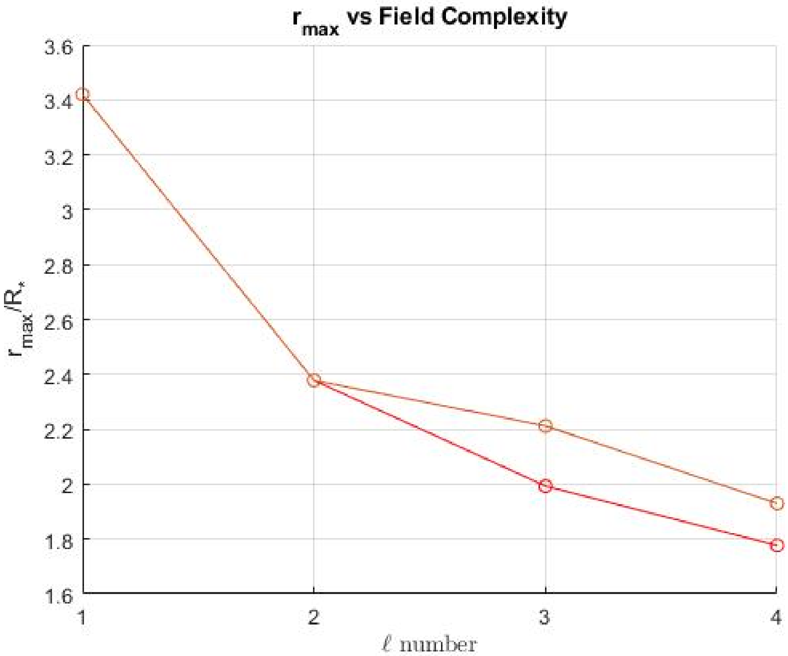

Figure 5.1: Figure shows how modelled maximum radial field extent at which the star's field can hold the X-ray emitting plasma r_{max} changes with increasing field complexity (increasing ℓ). Graph splits into two at $\ell > 2$ since the shells have multiple radial extents found in one quadrant of the star's model.

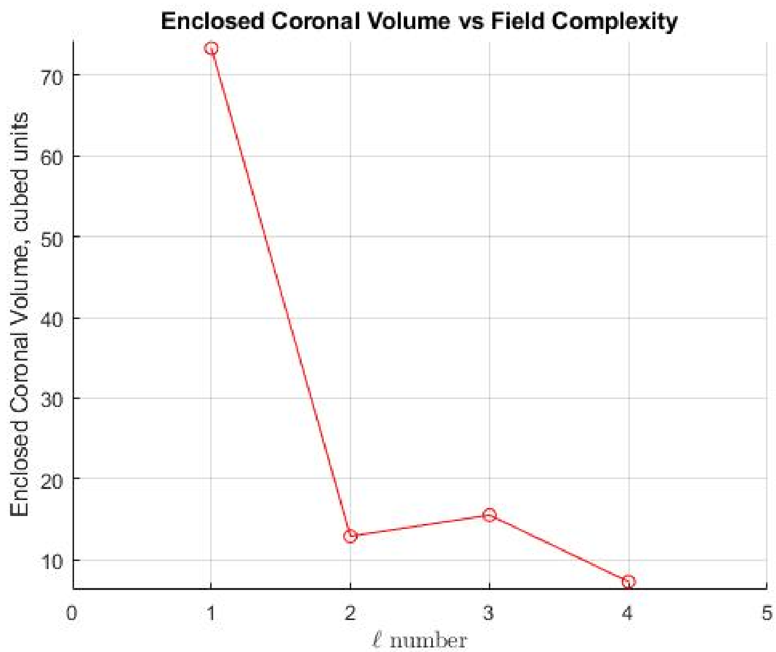

Figure 5.2: Figure shows how calculated X-ray emitting Volume changes with a increase in field complexity (increasing ℓ).

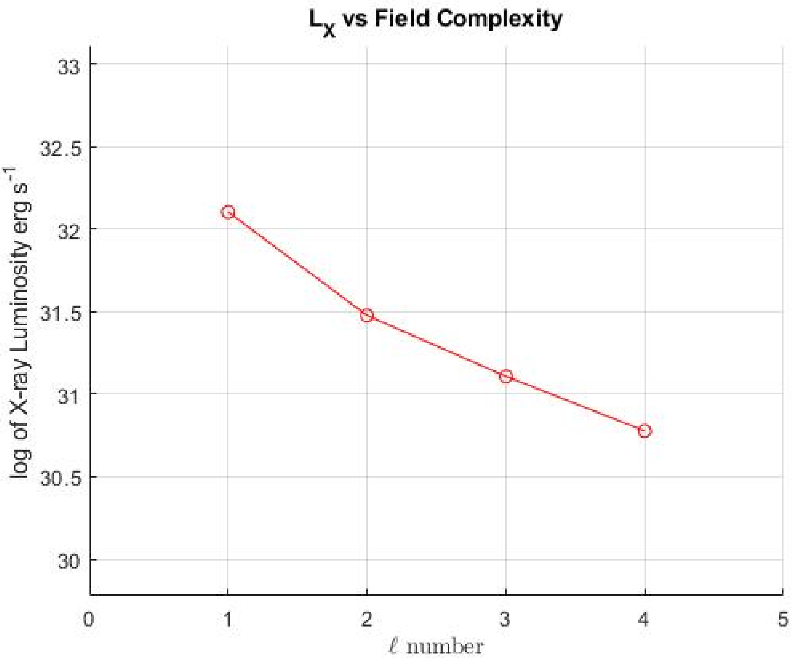

Figure 5.3: Figure shows how calculated X-ray luminosity changes with field complexity ℓ.

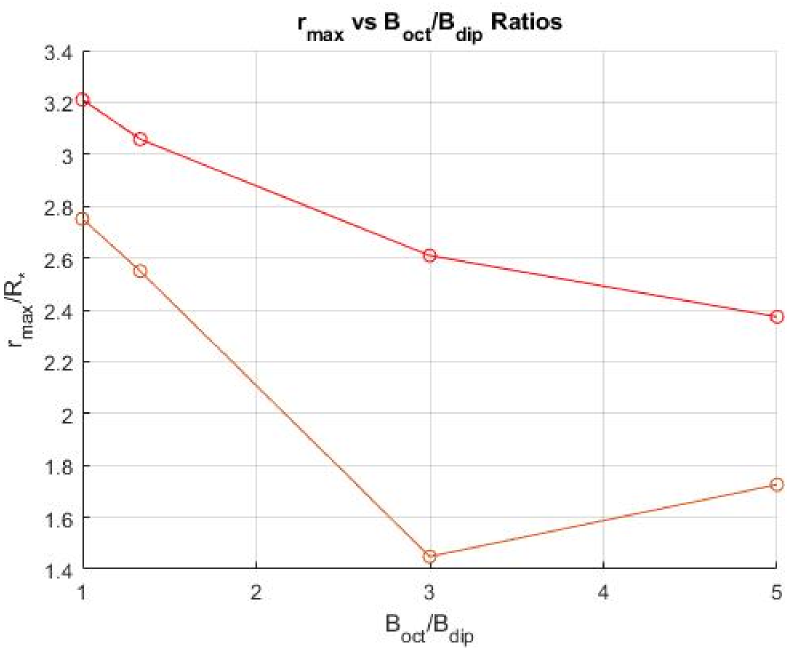

Figure 5.4: Figure shows how different B_{oct}/B_{dip} ratios change with maximum radial field extent at which the star's field can hold the X-ray emitting plasma r_{max} in combination field configurations.

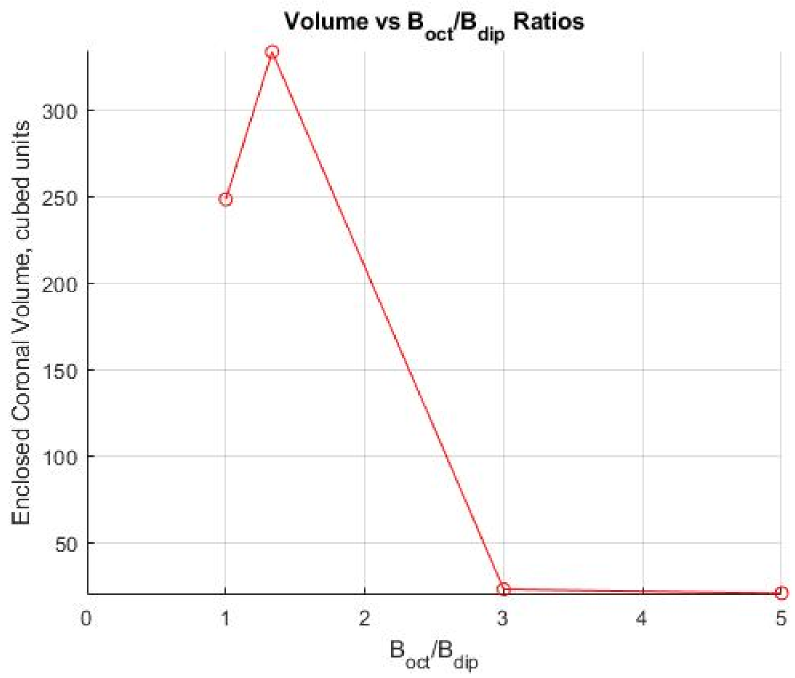

Figure 5.5: Figure shows how different B_{oct}/B_{dip} ratios changes with X-ray emitting volume.

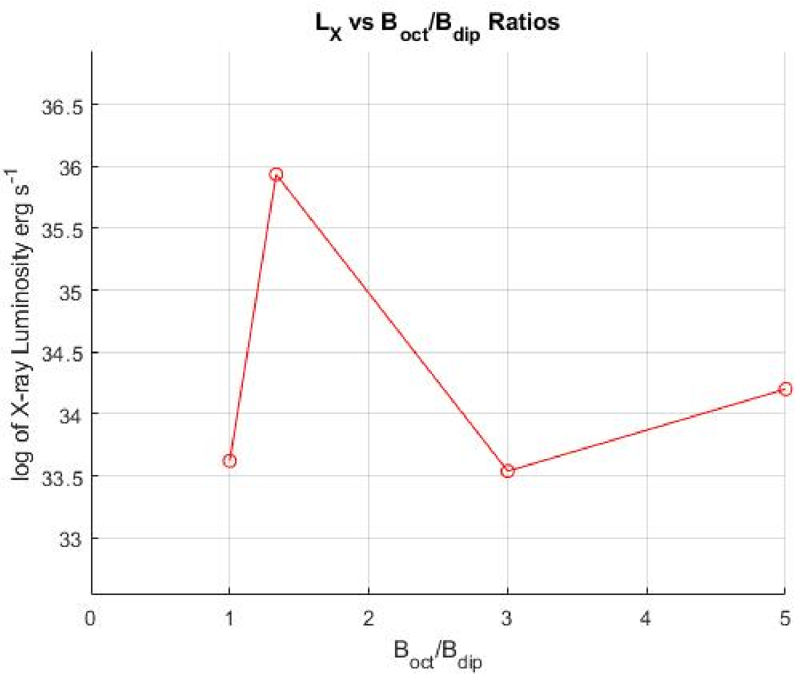

Figure 5.6: Figure shows how different B_{oct}/B_{dip} ratios changes with calculated X-ray luminosity.

6 Discussion and conclusions

The COUP Data used for observations into PMS star's included 148 star's with radiative cores in the PMS sequence, 836 fully convective star's, only 57 Henyey track star's and 927 Hayashi track star's (Gregory et al. 2016). The size of the data for radiative core samples and Henyey track star's compared to Hayashi track and fully convective star's were unexpected since the PMS clusters observed were relatively young, and should have a higher proportion of low-mass (younger PMS star's) to high-mass star's (older PMS star's) (Gregory et al. 2016). Figures 2.6, 2.7, 2.8 and 2.9 in section §2.1 show a slight negative relationship or said 'decay' in X-ray luminosity with age for mainly Hayashi track star's. Gregory et al. (2016) shows a slight sub linear relationship between stellar luminosity and x-ray luminosity for fully convective PMS star's has been observed and calculated to give $L_X \propto L_*^{0.93\pm0.04}$, the exponent for Hayashi track star's with developing radiative cores has a reduced value of 0.61 ± 0.08. The exponent is further reduced to 0.33 ± 0.09 for star's with partially convective interiors and star's on the Henyey track which have radiative interiors, This exponent can conclude there is no correlation between L_X and L_* for the observed Henyey track star's (Gregory et al. 2016). The observed difference in the exponents can help the case of theorised decay in X-ray emission from young star's with the development of a radiative core. This is the case due to the radiative cores effect of the star's magnetic field configuration discussed in section §1, we test how the magnetic field configuration determines the majorly coronal X-ray emission from a star (Güdel 2009). The formation of the star's radiative core increases the complexity of the star's magnetic field configuration (Gregory et al. 2014), to test the magnetic field configurations effect on the X-ray emission I modelled multiple stellar magnetic field configurations with set parameters to isolate the relationship.

Section §2.2 describes the X-rays luminosity's relationship to the enclosed X-ray emitting volume that's directly influenced by the change in field complexity, §3.1 shows how we would describe the field topology and implement that into the equations that describes the X-rays luminosity (1). This implementation is described by the differences between the plots 3.2, 3.3, 3.4 and 3.5, where we define the X-ray emitting volume as the area under r_{max} (red line) converted into a volume assuming even azimuthal dependency across the star ($d\phi = 0$). To calculate the X-ray luminosity for each of the mentioned magnetic field configuration models and support the speculation of their 'decaying' relationship, the emission measure found in equation 1 and described by equation 6 has to be determined by the X-ray emitting volume which is calculated numerically in my code using the configuration models in section §3.1 and creating results shown in 3.2. Calculations of the X-ray luminosity as seen in Figure 5.2 supports the speculation that an increasing magnetic field complexity (increasing ℓ number) would decrease the total X-ray emitting volume of the star, in turn decreasing the calculated L_X from that volume considering the relationship in equation 1, Figure 5.3 shows this graphically. Gregory et al. (2014) argues that the formation of the radiative core causes an increase in the stars magnetic field complexity. The formation of radiative core occurs as the star evolves along the Hayashi track signalled by the fact that star's found on the Henyey track already have substantial radiative cores (Gregory et al. 2014). Therefore as a star evolves along the Hayashi track (increasing age) their magnetic fields become more complex (increasing ℓ) which decreases their coronal X-ray emission (which makes the majority of the stars X-ray emission (Gregory et al. 2014)) explaining the "decay" of X-ray emission in PMS star's shown in Figures 2.6, 2.7, 2.8 and 2.9.

To further support the speculation that an increasing magnetic field complexity would decrease a star's Coronal X-ray emission, we looked to model field topology's with more than one magnetic field component and further increase the complexity of the magnetic field. Using a dipole+octupole field configuration ($\ell = 1 and \ell = 3$) with an increasing B_{oct}/B_{dip} ratio to simulate a further increase in magnetic field complexity, we then calculate the X-ray luminosity for different B_{oct}/B_{dip} ratios and test to find the same decrease in L_X seen in Figure 5.3 and Table 5.1. My results for the calculated L_X in combination multipoles are shown in Figure 5.6 and Table 5.2, that don't show the same results which makes me think that my code for the dipole+octupole field configuration needs more further work. I would try and get the code to recognise the existance of the null point and not count the area underneath it as apart of the X-ray emitting volume which would decrease the emission measure values seen in Table 4.3 to a reasonable magnitude allowing me to isolate the cause of the unexpected inconsistent L_X values seen in figure 5.6. Once this problem is resolved i would test other ℓ combination field configurations to see if they behave the same way as the dipole+octupole results with increasing **B**-field strength component ratios, this would also allow me to add different combinations of ℓ numbers with their associated L_X values to Figure 5.3.

In conclusion my calculated X-ray luminosity's in Table 5.1 are consistent with what we would see in typical $0.5M_\odot$ PMS star's as seen in Figures 2.6, 2.7, 2.8 and 2.9. The results also show the speculated decrease in X-ray luminosity with increasing field complexity as shown in Figure 5.3, despite the unexpectedly small X-ray emitting volume of $\ell = 2$ as shown in Figure 5.2, that should be greater than the calculated volume of $\ell = 3$ to remain consistent with its corresponding calculated L_X value in Figure 5.3. It cannot be said that results belonging to the dipole+octupole combination field topology supported the speculated decrease in L_X like the previous results. These combination magnetic field models tried to stimulate an increase in field complexity with an increasingly dominant octupole field component (increasing B_{oct}/B_{dip} ratio), I would argue that this would be due to errors in my code due to the existence of the null point in section §4 and therefore that these results should not be used to argue against the speculated decrease in L_X with increasing field complexity.

References

Adams F. C., Gregory S. G., 2012, ApJ, 744, 55

Aschwanden M. J., Stern R. A., Güdel M., 2008, ApJ, 672, 659

Chabrier G., Baraffe I., 1997, A&A, 327, 1039

Davies C. L., 2015, PhD thesis, University of St. Andrews

Donati J. F., Semel M., Carter B. D., Rees D. E., Collier Cameron A., 1997, MNRAS, 291, 658

Donati J. F., Jardine M. M., Gregory S. G., Petit P., Bouvier J., Dougados C., Ménard F., Collier Cameron A., Harries T. J., Jeffers S. V., Paletou F., 2007, MNRAS, 380, 1297

Donati J.-F., Gregory S. G., Montmerle T., Maggio A., Argiroffi C., Sacco G., Hussain G., Kastner J., Alencar S. H. P., Audard M., Bouvier J., Damiani F., Güdel M., Huenemoerder D., Wade G. A., 2011, MNRAS, 417, 1747

Favata F., Flaccomio E., Reale F., Micela G., Sciortino S., Shang H., Stassun K. G., Feigelson E. D., 2005, ApJS, 160, 469

Folsom C. P., Petit P., Bouvier J., Lèbre A., Amard L., Palacios A., Morin J., Donati J. F., Jeffers S. V., Marsden S. C., Vidotto A. A., 2016, MNRAS, 457, 580

Garren D. A., Chen J., 1994, Physics of Plasmas, 1, 3425

Getman K. V., Flaccomio E., Broos P. S., Grosso N., Tsujimoto M., Townsley L., Garmire G. P., Kastner J., Li J., Harnden F. R. J., Wolk S., Murray S. S., Lada C. J., Muench A. A., McCaughrean M. J., Meeus G., Damiani F., Micela G., Sciortino S., Bally J., Hillenbrand L. A., Herbst W., Preibisch T., Feigelson E. D., 2005, ApJS, 160, 319

Gregory S. G., Donati J. F., 2011, Astronomische Nachrichten, 332, 1027

Gregory S. G., Jardine M., Simpson I., Donati J. F., 2006, MNRAS, 371, 999

Gregory S. G., Jardine M., Gray C. G., Donati J. F., 2010, Reports on Progress in Physics, 73, 126901

Gregory S. G., Donati J. F., Morin J., Hussain G. A. J., Mayne N. J., Hillenbrand L. A., Jardine M., 2014, in Petit P., Jardine M., Spruit H. C., eds, Vol. 302, Magnetic Fields throughout Stellar Evolution. pp 40–43 (arXiv:1309.7556), doi:10.1017/S1743921314001677

Gregory S. G., Adams F. C., Davies C. L., 2016, MNRAS, 457, 3836

Güdel M., 2009, Physics of Stellar Coronae. p. 269, doi:10.1007/978-3-642-00210-6˙8

Hudson H. S., Kosugi T., 1999, Science, 285, 849

Jardine M., Wood K., Collier Cameron A., Donati J. F., Mackay D. H., 2002, MNRAS, 336, 1364

Johnstone C. P., Jardine M., Gregory S. G., Donati J. F., Hussain G., 2014, MNRAS, 437, 3202

Larson R. B., 2003, Reports on Progress in Physics, 66, 1651

Muzerolle J., Calvet N., Hartmann L., 2001, ApJ, 550, 944

Piddington J. H., 1983, Ap&SS, 90, 217

Stahler S. W., 1983, ApJ, 274, 822

Stassun K., Ardila D., Matt S., Feigelson E., 2006, in American Astronomical Society Meeting Abstracts. p. 219.06

Appendix

```
%Physics Project Task 3
clc;
clear all;
clf;
dbstop if error

data = load('moredata.txt');

for i = 1:11
    for j = 1:length(data)
        if data(j,i) == 999.9900
            data(j,:) = NaN;
        elseif data(j,i) == 99.9900
```

```
            data(j,:) = NaN;
        end
    end
end

kT1 = data(:,1);
kT1 = kT1*1e3*(1.6*1e-19)/(1.381*1e-23)/(1e6);

kT1_e = data(:,2);
kT1_e = kT1_e*1e3*(1.6*1e-19)/(1.381*1e-23)/(1e6);

kT2 = data(:,3);
kT2 = kT2*1e3*(1.6*1e-19)/(1.381*1e-23)/(1e6);

kT2_e = data(:,4);
kT2_e = kT2_e*1e3*(1.6*1e-19)/(1.381*1e-23)/(1e6);

Ls = data(:,5);

Lh = data(:,6);

Lhc = data(:,7);

Lt = data(:,8);

Ltc = data(:,9);

L = (data(:,5) + data(:,6) + data(:,7) + data(:,8) + data(:,9))/5;

Mass = data(:,10);

Age = data(:,11);

average_kT2 = mean(kT2,'omitnan')
median_kT2 = median(kT2,'omitnan')

for i = 1:length(kT2)
    MAD(i) = ((kT2(i)-median_kT2)^2)^0.5;
end
MAD_kT2 = sum(MAD,'omitnan')

figure(1)
ax = gca;
hold (ax,'on')
ylabel(ax,'Temperature (Kelvin, K) *10^6');
```

```
xlabel(ax,'Solar Mass');
% errorbar(ax,kT2,Mass,kT2_e)
scatter(ax,Mass,kT2)
mean_temperature = yline(ax,average_kT2,'-.b','DisplayName','Mean ...
    Temperature');
median_temperature = yline(ax,median_kT2,'-.r','DisplayName','Median ...
    Temperature');
legend([mean_temperature,median_temperature])
title('Coronal Temperature vs Mass')
axis([0.1 3 0 18*10^(7)/(1e6)])
hold (ax,'off')

figure(2)
bx = gca;
hold (bx,'on')
ylabel(bx,'Temperature (Kelvin, K) *10^6');
xlabel(bx,'Age, log(Years, yr)');
% errorbar(bx,kT2,Age,kT2_e)
scatter(bx,Age,kT2)
mean_temperature = yline(bx,average_kT2,'-.b','DisplayName','Mean ...
    Temperature');
median_temperature = yline(bx,median_kT2,'-.r','DisplayName','Median ...
    Temperature');
legend([mean_temperature,median_temperature])
title('Coronal Temperature vs Age')
axis([4 8 0 12*10^(7)/(1e6)])
hold (bx,'off')

% linkaxes([ax1,ax2,ax3,ax4],'x','y');
% ylabel(t,'X-ray Luminosity, log[L_X] W');
% xlabel(t,'Age, log(Years, yr)');
% title(t,'X-ray Luminosity vs Age')


figure(3)
ax = gca;
hold (ax,'on')
ylabel(ax,'X-ray Luminosity, log[L_X] W');
xlabel(ax,'Solar Mass');
% errorbar(ax,kT2,Mass,kT2_e)
scatter(ax,Mass,L)
mean_luminosity = yline(bx,mean(L,'omitnan'),'-.b','DisplayName','Mean L_X');
median_luminosity = ...
    yline(bx,median(L,'omitnan'),'-.r','DisplayName','Median L_X');
legend([mean_luminosity,median_luminosity])
```

```
title('X-ray Luminosity vs Mass')
axis([0 3 28 32])
hold (ax,'off')

figure(4)
ax = gca;
hold (ax,'on')
ylabel(ax,'X-ray Luminosity, log[L_X] W');
xlabel(ax,'Solar Mass');
% errorbar(ax,kT2,Mass,kT2_e)
scatter(ax,Mass,L)
mean_luminosity = yline(bx,mean(L,'omitnan'),'-.b','DisplayName','Mean L_X');
median_luminosity = ...
    yline(bx,median(L,'omitnan'),'-.r','DisplayName','Median L_X');
legend([mean_luminosity,median_luminosity])
title('X-ray Luminosity vs Mass')
axis([0 1 28 32])
hold (ax,'off')

figure(5)
bx = gca;
hold (bx,'on')
xlabel(bx,'Temperature (Kelvin, K) *10^6');
ylabel(ax,'X-ray Luminosity, log[L_X] W');
% errorbar(bx,kT2,Age,kT2_e)
scatter(bx,kT2,L)
mean_luminosity = yline(bx,mean(L,'omitnan'),'-.b','DisplayName','Mean L_X');
median_luminosity = ...
    yline(bx,median(L,'omitnan'),'-.r','DisplayName','Median L_X');
legend([mean_luminosity,median_luminosity])
title('X-ray Luminosity vs Coronal Temperature')
axis([0 80 28 32])
hold (bx,'off')
```

```
%Physics Project Task 1
%lth order multipole
clc
clear all
clf
dbstop if error
%clearing console, and entering debug mode on error

Bpole_1 = 1000;%feild strength of star
```

```
Bpole_2 = 5000;
M_Sun = 1.988*10^33;%mass of sun in grams
P_rot = 5*24*60*60; %in seconds CP Johnstone 2013
G = 6.67*10^(-8);%gravitational constant in grams
M = 0.5*M_Sun;%mass of star
T = 1*10^7;%coronal temperature in kelvin
k_B = 1.3807*10^(-16);%boltzman constant
umH = 10^(-24);%mass of hydrogen molecule in kelvin
cs = (k_B*T/umH)^0.5;%constant cs
k = 10^(-5); %CP Johnstone 2013

R = 1;%radius of star in units of r/Rstar
R_Sun = 6.957*10^10;%radius of sun, wiki in cm ?
R_Star = 2*R_Sun;%radius of star in cm ?

w = 2*pi/P_rot;%radial period omega
phig = G*M/R_Star/cs^2;%constant phi gravitational
phic = 0.5*(w*R_Star/cs)^2;%constant phi coronal ?

p0_1 = 0;
p0_2 = 0;
n = 10000;%max index, iteration limit, size of data matrices
ds = 10^(-2);%integration step size along each field line

%plotting star's surface
figure(1)
ax = gca;
hold (ax,'on')
grid (ax,'on')
xlabel(ax,'x/R_*')
ylabel(ax,'z/R_*')
title('B_{oct}/B_{dip} = 1 Field Configuration')

l_1 = 1;%lth order value representing type of field configuration star has
%eg 1 is dipole, 2 is quadripole etc.
syms cX sX X %defining symbols used to create legendre polynomials for given
%l number
%cX represents cos(x)
%sX represents sin(x)
%X represents x
Pl_1 = legendreP(l_1,cX);%legendre polynomail function
Plm_1 = diff(sX*Pl_1,cX);%differentiating with respect to cos(x)
Pl_1 = subs(Pl_1,cX,cos(X));%subbing cX for cos(x)
Plm_1 = subs(Plm_1,cX,cos(X));
Plm_1 = subs(Plm_1,sX,sin(X));%subbing sX for sin(x)
```

```
eqn = Pl_1 == 0;%equating to 0 to finds roots
S_1 = eval(solve(eqn));%solving for roots of legendre

%creating and solving the legendre polynomials for the second l-th order
%multipole, repeating calculations from before but with another l number
l_2 = 3;
syms cX sX X
Pl_2 = legendreP(l_2,cX);%1st legendre polynomial
Plm_2 = diff(sX*Pl_2,cX);%2nd legendre polynomial
%subbing cos(X) and sin(X) into symbols
Pl_2 = subs(Pl_2,cX,cos(X));
Plm_2 = subs(Plm_2,cX,cos(X));
Plm_2 = subs(Plm_2,sX,sin(X));

eqn = Pl_2 == 0;
S_2 = eval(solve(eqn));

S = [S_2',S_1'];%combining routes of and removing routes outside of ...
    positive axis
for s = 1:length(S)
    if S(s) < 0
        S(s) = abs(S(s)) + pi/2;%removing roots outside of range 0 to pi
    end
end
S(S>pi/2)=[];
S = unique(S);%removing repeating roots

syms Xi f g l Bpole%defining more symbols for calculations of B field r ...
    and theta components
Br = Bpole*(1/Xi)^(l+2)*f; %radial component of B field strength
Bt = Bpole/(l+1)*(1/Xi)^(l+2)*g;%thetal component of B field strength

p_mag_1_axis = [];%creating lists to store gas pressure and magnetic ...
    pressure under rmax
p_gas_1_axis = [];
rmax_axis = [];%for values along x axis from R to rmax
rmax_temp = zeros(1,length(S));%matrix for temperary values of rmax
%stores values of r for each field line being plotted
rmax_temp(rmax_temp==0) = R+0.1;%r value of first
rmax_prev = zeros(1,length(S));%r values of the previous field line
rmax_prev(rmax_prev==0) = R;
iteration_counter = [];

E = 0;
V = 0;%volume under rmax
```

```
pcheck = zeros(1,length(S));%this defines the characteristic of each ...
    feild line
rmax_max = zeros(1,length(S));
%0 is for normal closed field line under rmax
%1 is rmax
%2 is open field lines above rmax
%3 is used to break the while loop when rmax has been plotted

while sum(pcheck)/length(pcheck) < 3

t1_footpoint = zeros(1,length(S));
r1_footpoint = zeros(1,length(S));
t2_footpoint = zeros(1,length(S));
r2_footpoint = zeros(1,length(S));

for s = 1:length(S)%iterating over the roots of the legendre polynomials
%creates arbitrary starting points for iteration for each field
%line

p_mag_1 = zeros(1,n);%creating empty matrices for magnetic pressure
p_mag_2 = zeros(1,n);

p_gas_1 = zeros(1,n);%creating empty matrices for gas pressure
p_gas_2 = zeros(1,n);

t1 = zeros(1,n);%theta values of field lines
t2 = zeros(1,n);

t1(1) = S(s);%beginning theta values for iteration
t2(1) = S(s);

E1 = zeros(1,n);
E2 = zeros(1,n);

%this is why we need 2 matrices for each parameter being calculated
%since we are staring iteration at the roots of the legendre (apex
%theta value of each field line) we then calculate everything in
%both directions working down the field lines from the apex until
%we reach the star's surface or either axis.

r1 = zeros(1,n);%radial coords
r2 = zeros(1,n);

r1(1) = rmax_temp(s);%beggining radial coord as temperary rmax
r2(1) = rmax_temp(s);
```

```
tr1_check = 0;%checks if theta is between 0 and pi/2 or if r is above R ...
    of star
tr2_check = 0;
%reseting pcheck for each field line

for j = 1:n %iterating over each defined matrix
    %evaluating each legendre polynomial with theta values
    f1_1 = subs(Pl_1,X,t1(j));
    g1_1 = subs(Plm_1,X,t1(j));
    f1_2 = subs(Pl_1,X,t2(j));
    g1_2 = subs(Plm_1,X,t2(j));
    f2_1 = subs(Pl_2,X,t1(j));
    g2_1 = subs(Plm_2,X,t1(j));
    f2_2 = subs(Pl_2,X,t2(j));
    g2_2 = subs(Plm_2,X,t2(j));

    %dimentionless constant epsilon ?
    Xi1 = r1(j)/R;
    Xi2 = r2(j)/R;

    %evaluating radial component for B field strength
    Br1 = subs(Br,Xi,Xi1);
    Br1_1 = subs(Br1,Bpole,Bpole_1);
    Br1_1 = subs(Br1_1,l,l_1);
    Br2_1 = subs(Br1,Bpole,Bpole_2);
    Br2_1 = subs(Br2_1,l,l_2);
    Br1 = eval(subs(Br1_1,f,f1_1) + subs(Br2_1,f,f2_1));

    Bt1 = subs(Bt,Xi,Xi1);
    Bt1_1 = subs(Bt1,Bpole,Bpole_1);
    Bt1_1 = subs(Bt1_1,l,l_1);
    Bt2_1 = subs(Bt1,Bpole,Bpole_2);
    Bt2_1 = subs(Bt2_1,l,l_2);
    Bt1 = eval(subs(Bt1_1,g,g1_1) + subs(Bt2_1,g,g2_1));

    %calculating magnitude of B field
    B1_mag = (Br1^2+Bt1^2)^0.5;

    Br2 = subs(Br,Xi,Xi2);
    Br1_2 = subs(Br2,Bpole,Bpole_1);
    Br1_2 = subs(Br1_2,l,l_1);
    Br2_2 = subs(Br2,Bpole,Bpole_2);
    Br2_2 = subs(Br2_2,l,l_2);
    Br2 = eval(subs(Br1_2,f,f1_2) + subs(Br2_2,f,f2_2));
```

```
    Bt2 = subs(Bt,Xi,Xi2);
    Bt1_2 = subs(Bt2,Bpole,Bpole_1);
    Bt1_2 = subs(Bt1_2,l,l_1);
    Bt2_2 = subs(Bt2,Bpole,Bpole_2);
    Bt2_2 = subs(Bt2_2,l,l_2);
    Bt2 = eval(subs(Bt1_2,g,g1_2) + subs(Bt2_2,g,g2_2));

    B2_mag = (Br2^2+Bt2^2)^0.5;

    %calculating change in r and theta
    dr1 = -Br1*ds/B1_mag;
    dt1 = -Bt1*ds/r1(j)/B1_mag;
    dr2 = Br2*ds/B2_mag;
    dt2 = Bt2*ds/r2(j)/B2_mag;

    %calculating new r and theta coords
    r1(j+1) = r1(j) + dr1;
    t1(j+1) = t1(j) + dt1;
    r2(j+1) = r2(j) + dr2;
    t2(j+1) = t2(j) + dt2;

    %checking if r is below R
    if r1(j+1) < R
        t1(j+1) = t1(j);
        r1(j+1) = R;
        tr1_check = 1;

        t1_footpoint(s) = t1(j+1);
        r1_footpoint(s) = r1(j+1);

        f1_1 = subs(Pl_1,X,t1_footpoint(s));
        g1_1 = subs(Plm_1,X,t1_footpoint(s));
        f2_1 = subs(Pl_2,X,t1_footpoint(s));
        g2_1 = subs(Plm_2,X,t1_footpoint(s));

        Br0 = subs(Br,Xi,r1_footpoint(s)/R);
        Br0_1 = subs(Br0,Bpole,Bpole_1);
        Br0_1 = subs(Br0_1,l,l_1);
        Br0_2 = subs(Br0,Bpole,Bpole_2);
        Br0_2 = subs(Br0_2,l,l_2);
        Br0 = eval(subs(Br0_1,f,f1_1) + subs(Br0_2,f,f2_1));

        Bt0 = subs(Bt,Xi,r1_footpoint(s)/R);
        Bt0_1 = subs(Bt0,Bpole,Bpole_1);
```

```
            Bt0_1 = subs(Bt0_1,l,l_1);
            Bt0_2 = subs(Bt0,Bpole,Bpole_2);
            Bt0_2 = subs(Bt0_2,l,l_2);
            Bt0 = eval(subs(Bt0_1,g,g1_1) + subs(Bt0_2,g,g2_1));

            p0_1 = k*(Br0^2+Bt0^2);
        end

        if r2(j+1) < R
           t2(j+1) = t2(j);
           r2(j+1) = R;
           tr2_check = 1;

           t2_footpoint(s) = t2(j+1);
           r2_footpoint(s) = r2(j+1);

           f1_2 = subs(Pl_1,X,t2_footpoint(s));
           g1_2 = subs(Plm_1,X,t2_footpoint(s));
           f2_2 = subs(Pl_2,X,t2_footpoint(s));
           g2_2 = subs(Plm_2,X,t2_footpoint(s));

           Br0 = subs(Br,Xi,r2_footpoint(s)/R);
           Br0_1 = subs(Br0,Bpole,Bpole_1);
           Br0_1 = subs(Br0_1,l,l_1);
           Br0_2 = subs(Br0,Bpole,Bpole_2);
           Br0_2 = subs(Br0_2,l,l_2);
           Br0 = eval(subs(Br0_1,f,f1_2) + subs(Br0_2,f,f2_2));

           Bt0 = subs(Bt,Xi,r2_footpoint(s)/R);
           Bt0_1 = subs(Bt0,Bpole,Bpole_1);
           Bt0_1 = subs(Bt0_1,l,l_1);
           Bt0_2 = subs(Bt0,Bpole,Bpole_2);
           Bt0_2 = subs(Bt0_2,l,l_2);
           Bt0 = eval(subs(Bt0_1,g,g1_2) + subs(Bt0_2,g,g2_2));

           p0_2 = k*(Br0^2+Bt0^2);
        end

        %checking if theta is in range of 0 to pi
        if t1(j+1) < 0
            t1(j+1) = 0;
            r1(j+1) = r1(j);
            tr1_check = 1;
            p0_1 = p0_2;
        end
```

```
    if t1(j+1) > pi/2
        t1(j+1) = pi/2;
        r1(j+1) = r1(j);
        tr1_check = 1;
        p0_1 = p0_2;
    end
    if t2(j+1) < 0
        t2(j+1) = 0;
        r2(j+1) = r2(j);
        tr2_check = 1;
        p0_2 = p0_1;
    end
    if t2(j+1) > pi/2
        t2(j+1) = pi/2;
        r2(j+1) = r2(j);
        tr2_check = 1;
        p0_2 = p0_1;
    end
    %breaking when field lines are complete
    if tr1_check == 1
        if tr2_check == 1
            break
        end
    end
end

iteration_counter = [iteration_counter,j];

figure(1)

B1 = zeros(1,n);%magnitude of B field strength
B2 = zeros(1,n);
B1(B1==0) = NaN;
B2(B2==0) = NaN;

for b = 1:j
    Xi1 = r1(b)/R;
    Xi2 = r2(b)/R;

    f1_1 = subs(Pl_1,X,t1(b));
    g1_1 = subs(Plm_1,X,t1(b));
    f1_2 = subs(Pl_1,X,t2(b));
    g1_2 = subs(Plm_1,X,t2(b));
    f2_1 = subs(Pl_2,X,t1(b));
    g2_1 = subs(Plm_2,X,t1(b));
```

```
    f2_2 = subs(Pl_2,X,t2(b));
    g2_2 = subs(Plm_2,X,t2(b));

    Br1 = subs(Br,Xi,Xi1);
    Br1_1 = subs(Br1,Bpole,Bpole_1);
    Br1_1 = subs(Br1_1,l,l_1);
    Br2_1 = subs(Br1,Bpole,Bpole_2);
    Br2_1 = subs(Br2_1,l,l_2);

    Br1 = eval(subs(Br1_1,f,f1_1) + subs(Br2_1,f,f2_1));

    Bt1 = subs(Bt,Xi,Xi1);
    Bt1_1 = subs(Bt1,Bpole,Bpole_1);
    Bt1_1 = subs(Bt1_1,l,l_1);
    Bt2_1 = subs(Bt1,Bpole,Bpole_2);
    Bt2_1 = subs(Bt2_1,l,l_2);

    Bt1 = eval(subs(Bt1_1,g,g1_1) + subs(Bt2_1,g,g2_1));

    B1(b) = (Br1^2+Bt1^2)^0.5;

    Br2 = subs(Br,Xi,Xi2);
    Br1_2 = subs(Br2,Bpole,Bpole_1);
    Br1_2 = subs(Br1_2,l,l_1);
    Br2_2 = subs(Br2,Bpole,Bpole_2);
    Br2_2 = subs(Br2_2,l,l_2);

    Br2 = eval(subs(Br1_2,f,f1_2) + subs(Br2_2,f,f2_2));

    Bt2 = subs(Bt,Xi,Xi2);
    Bt1_2 = subs(Bt2,Bpole,Bpole_1);
    Bt1_2 = subs(Bt1_2,l,l_1);
    Bt2_2 = subs(Bt2,Bpole,Bpole_2);
    Bt2_2 = subs(Bt2_2,l,l_2);

    Bt2 = eval(subs(Bt1_2,g,g1_2) + subs(Bt2_2,g,g2_2));

    B2(b) = (Br1^2+Bt1^2)^0.5;

    %magnetic pressure from field line calculation
    p_mag_1(b) = B1(b)^2/8/pi;
    p_mag_2(b) = B2(b)^2/8/pi;

    %gas pressure calculations
    q1 = sin(t1(b))^2/Xi1;
```

```
    q2 = sin(t2(b))^2/Xi2;

    p_gas_1(b) = p0_1*exp(phig*(1/Xi1-1)+phic*q1*(Xi1^3-1));
    p_gas_2(b) = p0_2*exp(phig*(1/Xi2-1)+phic*q2*(Xi2^3-1));

    if pcheck(s) ≠ 1
        p_gas_1(b)
        p_gas_2(b)
        B1(b)
        B2(b)
        if or(p_gas_1(b)/p_mag_1(b) ≥ 1,p_gas_2(b)/p_mag_2(b) ≥ 1) == 1
            if abs(rmax_temp(s)-rmax_max(s)) ≤ ds/10
                pcheck(s) = 1;
            elseif rmax_temp(s) == rmax_prev(s)
                pcheck(s) = 1;
            else
                pcheck(s) = 2;
                rmax_max(s) = rmax_temp(s);
                rmax_temp(s) = rmax_prev(s)
                break
            end
        elseif pcheck(s) == 2
            rmax_prev(s) = rmax_temp(s);
            rmax_temp(s) = (rmax_temp(s) + rmax_max(s))/2
            break
        end
    end

    if pcheck(s) == 1%if rmax has been found
        dr1grid = abs(diff([r1(b),r1(b+1)]));
        dr2grid = abs(diff([r2(b),r2(b+1)]));
        dtheta1grid = abs(diff([t1(b),t1(b+1)]));
        dtheta2grid = abs(diff([t2(b),t2(b+1)]));
        theta1grid = t1(b):dtheta1grid:S(s);
        theta2grid = t2(b):dtheta2grid:S(s);

        for i = 1:numel(theta1grid)
            V = V + abs(r1(b)^2*sin(theta1grid(i))*dtheta1grid*4*pi*dr1grid);
            E = E + ...
               abs(r1(b)^2*sin(theta1grid(i))*dtheta1grid*4*pi*dr1grid*p_gas_1(b)^2);
        end
        for i = 1:numel(theta2grid)
            V = V + abs(r2(b)^2*sin(theta2grid(i))*dtheta2grid*4*pi*dr2grid);
            E = E + ...
               abs(r2(b)^2*sin(theta2grid(i))*dtheta2grid*4*pi*dr2grid*p_gas_2(b)^2);
```

```
            end

%           figure(1)
%           ...
    plot([R*sin(t1(b)),r1(b)*sin(t1(b))],[R*cos(t1(b)),r1(b)*cos(t1(b))],'g')
%           ...
    plot([R*sin(t2(b)),r2(b)*sin(t2(b))],[R*cos(t2(b)),r2(b)*cos(t2(b))],'g')

        end
        %saving gas and magnetic pressure values for plot
        if t1(b) == pi/2
            p_gas_1_axis = [p_gas_1_axis,p_gas_1(b)];
            p_mag_1_axis = [p_mag_1_axis,p_mag_1(b)];
            rmax_axis = [rmax_axis,r1(b)];
        end
end

%calculating x and z coords
x1 = r1.*sin(t1);
z1 = r1.*cos(t1);
x2 = r2.*sin(t2);
z2 = r2.*cos(t2);
x1(x1==0)=NaN;%removing values equal to 0
z1(z1==0)=NaN;
x2(x2==0)=NaN;
z2(z2==0)=NaN;

if pcheck(s) == 1%if rmax has been found

    %combining data matrices for plots (dont work)
    t_max = [fliplr(t1),t2];
    B_max = [fliplr(B1),B2];
    r1(r1==0)=NaN;
    r2(r2==0)=NaN;
    r_max_r = [fliplr(r1),r2];

    %rmax plot
    figure(1)
    r_max = ...
        plot(ax,[x1,x2,x1,x2,-x1,-x2,-x1,-x2],[z1,z2,-z1,-z2,z1,z2,-z1,-z2],'-r','Displa

    %gas pressure and magnetic pressure plot
    figure(2)
    bx = gca;
    hold(bx,'on')
```

```
    beta_axis = p_gas_1_axis./p_mag_1_axis - 1;
    plot(rmax_axis,beta_axis,'r','DisplayName','\beta - 1')
    yline(0,'--')
    ylabel('\beta - 1')
    xlabel('r/R_*')
    title('\beta - 1 against \xi')%title
    hold(bx,'off')

    %Magnetic Field Strength plot
    figure(3)
    bx = gca;
    hold (bx,'on')
    plot(r_max_r,B_max,'b')
    ylabel('Magnetic Field Strength, B (Gauss)')
    xlabel('r/R_*')
    title('Magnitude of Magnetic Feild Strength With Distance From star's ...
        Surface')%title
    hold(bx,'off')

    %breaking while loop once rmax has been plotted
    pcheck(s) = 3;
end
if pcheck(s) == 0%if normal closed field line
    plot(ax,[x1,x2,x1,x2,-x1,-x2,-x1,-x2],[z1,z2,-z1,-z2,z1,z2,-z1,-z2],'-b');
    figure(1)
    %calculate new rmax temp
    rmax_prev(s) = rmax_temp(s);
    rmax_temp(s) = rmax_temp(s)+0.1;
end
end
end

if 10^5.75 < T < 10^6.3
    AT = 10^-21.94;
elseif 10^6.3 < T < 10^7.3
    AT = 10^-17.73*T^(-2/3);
elseif T > 10^7.3
    AT = 10^-21.94*T^(1/4);
end

%in cubic stellar radii into cm **stellar radius cubed
Lx = AT*E*R_Star^3/4/k_B^2/T^2;

disp(['numeric volume ',num2str(V)]) %displaying volume value
% disp(['analytic volume ...
```

```
    ',num2str(4*pi/3*rmax_temp^3*2/35*(1-1/rmax_temp)^1.5*(8 + ...
    12/rmax_temp + 15/rmax_temp^2))])
disp(['numeric rmax ',num2str(rmax_temp)])
disp(['numeric x-ray luminosity Lx ',num2str(Lx)])

figure(1)
theta_star = linspace(0,2*pi,60);%linspace of theta values used to plot star
xstar = cos(theta_star)*R;%x coordinates of the star
zstar = sin(theta_star)*R;%z coordinates of the star
Star = plot(ax,xstar,zstar,'-k','Linewidth',2,'DisplayName','Star');
axis equal
axis([-(max(r_max_r)) (max(r_max_r)) -(max(r_max_r)) ...
    (max(r_max_r))])%setting axis
set(gca,'FontSize',16)
set(gcf,'color','w');
print(gcf,'field.png','-dpng','-r600');
hold (ax,'off')%showing graph
```

```
%Physics Project Task 1
%lth order multipole
clc
clear all
clf
dbstop if error
%clearing console, and entering debug mode on error

Bpole_1 = 1000;%feild strength of star
Bpole_2 = 5000;
M_Sun = 1.988*10^33;%mass of sun in grams
P_rot = 5*24*60*60; %in seconds CP Johnstone 2013
G = 6.67*10^(-8);%gravitational constant in grams
M = 0.5*M_Sun;%mass of star
T = 1*10^7;%coronal temperature in kelvin
k_B = 1.3807*10^(-16);%boltzman constant
umH = 10^(-24);%mass of hydrogen molecule in kelvin
cs = (k_B*T/umH)^0.5;%constant cs
k = 10^(-5); %CP Johnstone 2013

R = 1;%radius of star in units of r/Rstar
R_Sun = 6.957*10^10;%radius of sun, wiki in cm ?
R_Star = 2*R_Sun;%radius of star in cm ?

w = 2*pi/P_rot;%radial period omega
```

```
phig = G*M/R_Star/cs^2;%constant phi gravitational
phic = 0.5*(w*R_Star/cs)^2;%constant phi coronal ?

p0_1 = 0;
p0_2 = 0;
n = 10000;%max index, iteration limit, size of data matrices
ds = 10^(-2);%integration step size along each field line

%plotting stars surface
figure(1)
ax = gca;
hold (ax,'on')
grid (ax,'on')
xlabel(ax,'x/R_*')
ylabel(ax,'z/R_*')
title('B_{oct}/B_{dip} = 1 Field Configuration')

l_1 = 1;%lth order value representing type of field configuration star has
%eg 1 is dipole, 2 is quadripole etc.
syms cX sX X %defining symbols used to create legendre polynomials for given
%l number
%cX represents cos(x)
%sX represents sin(x)
%X represents x
Pl_1 = legendreP(l_1,cX);%legendre polynomail function
Plm_1 = diff(sX*Pl_1,cX);%differentiating with respect to cos(x)
Pl_1 = subs(Pl_1,cX,cos(X));%subbing cX for cos(x)
Plm_1 = subs(Plm_1,cX,cos(X));
Plm_1 = subs(Plm_1,sX,sin(X));%subbing sX for sin(x)
eqn = Pl_1 == 0;%equating to 0 to finds roots
S_1 = eval(solve(eqn));%solving for roots of legendre

%creating and solving the legendre polynomials for the second l-th order
%multipole, repeating calculations from before but with another l number
l_2 = 3;
syms cX sX X
Pl_2 = legendreP(l_2,cX);%1st legendre polynomial
Plm_2 = diff(sX*Pl_2,cX);%2nd legendre polynomial
%subbing cos(X) and sin(X) into symbols
Pl_2 = subs(Pl_2,cX,cos(X));
Plm_2 = subs(Plm_2,cX,cos(X));
Plm_2 = subs(Plm_2,sX,sin(X));

eqn = Pl_2 == 0;
S_2 = eval(solve(eqn));
```

```
S = [S_2',S_1'];%combining routes of and removing routes outside of ...
    positive axis
for s = 1:length(S)
    if S(s) < 0
        S(s) = abs(S(s)) + pi/2;%removing roots outside of range 0 to pi
    end
end
S(S>pi/2)=[];
S = unique(S);%removing repeating roots

syms Xi f g l t BtBr Bpole%defining more symbols for calculations of B ...
    field r and theta components
Br = Bpole*(1/Xi)^(l+2)*f; %radial component of B field strength
Bt = Bpole/(l+1)*(1/Xi)^(l+2)*g;%thetal component of B field strength
J2 = 2*sin(t)^2*Xi;
J3 = 2*BtBr*sin(t)*cos(t)*Xi;

p_mag_1_axis = [];%creating lists to store gas pressure and magnetic ...
    pressure under rmax
p_gas_1_axis = [];
rmax_axis = [];%for values along x axis from R to rmax
rmax_temp = zeros(1,length(S));%matrix for temperary values of rmax
%stores values of r for each field line being plotted
rmax_temp(rmax_temp==0) = R+1;%r value of first
rmax_prev = zeros(1,length(S));%r values of the previous field line
rmax_prev(rmax_prev==0) = R;
iteration_counter = [];

E = 0;
V = 0;%volume under rmax
pcheck = zeros(1,length(S));%this defines the characteristic of each ...
    feild line
rmax_max = zeros(1,length(S));
%0 is for normal closed field line under rmax
%1 is rmax
%2 is open field lines above rmax
%3 is used to break the while loop when rmax has been plotted

while sum(pcheck)/length(pcheck) < 3

t1_footpoint = zeros(1,length(S));
r1_footpoint = zeros(1,length(S));
t2_footpoint = zeros(1,length(S));
r2_footpoint = zeros(1,length(S));
```

```
for s = 1:length(S)%iterating over the roots of the legendre polynomials
%creates arbitrary starting points for iteration for each field
%line

p_mag_1 = zeros(1,n);%creating empty matrices for magnetic pressure
p_mag_2 = zeros(1,n);

p_gas_1 = zeros(1,n);%creating empty matrices for gas pressure
p_gas_2 = zeros(1,n);

t1 = zeros(1,n);%theta values of field lines
t2 = zeros(1,n);

t1(1) = S(s);%beginning theta values for iteration
t2(1) = S(s);

E1 = zeros(1,n);
E2 = zeros(1,n);

%this is why we need 2 matrices for each parameter being calculated
%since we are staring iteration at the roots of the legendre (apex
%theta value of each field line) we then calculate everything in
%both directions working down the field lines from the apex until
%we reach the stars surface or either axis.

r1 = zeros(1,n);%radial coords
r2 = zeros(1,n);

r1(1) = rmax_temp(s);%beggining radial coord as temperary rmax
r2(1) = rmax_temp(s);

tr1_check = 0;%checks if theta is between 0 and pi/2 or if r is above R ...
    of star
tr2_check = 0;
%reseting pcheck for each field line

for j = 1:n %iterating over each defined matrix
    %evaluating each legendre polynomial with theta values
    f1_1 = subs(Pl_1,X,t1(j));
    g1_1 = subs(Plm_1,X,t1(j));
    f1_2 = subs(Pl_1,X,t2(j));
    g1_2 = subs(Plm_1,X,t2(j));
    f2_1 = subs(Pl_2,X,t1(j));
    g2_1 = subs(Plm_2,X,t1(j));
```

```
    f2_2 = subs(Pl_2,X,t2(j));
    g2_2 = subs(Plm_2,X,t2(j));

    %dimentionless constant epsilon ?
    Xi1 = r1(j)/R;
    Xi2 = r2(j)/R;

    %evaluating radial component for B field strength
    Br1 = subs(Br,Xi,Xi1);
    Br1_1 = subs(Br1,Bpole,Bpole_1);
    Br1_1 = subs(Br1_1,l,l_1);
    Br2_1 = subs(Br1,Bpole,Bpole_2);
    Br2_1 = subs(Br2_1,l,l_2);
    Br1 = eval(subs(Br1_1,f,f1_1) + subs(Br2_1,f,f2_1));

    Bt1 = subs(Bt,Xi,Xi1);
    Bt1_1 = subs(Bt1,Bpole,Bpole_1);
    Bt1_1 = subs(Bt1_1,l,l_1);
    Bt2_1 = subs(Bt1,Bpole,Bpole_2);
    Bt2_1 = subs(Bt2_1,l,l_2);
    Bt1 = eval(subs(Bt1_1,g,g1_1) + subs(Bt2_1,g,g2_1));

    %calculating magnitude of B field
    B1_mag = (Br1^2+Bt1^2)^0.5;

    Br2 = subs(Br,Xi,Xi2);
    Br1_2 = subs(Br2,Bpole,Bpole_1);
    Br1_2 = subs(Br1_2,l,l_1);
    Br2_2 = subs(Br2,Bpole,Bpole_2);
    Br2_2 = subs(Br2_2,l,l_2);
    Br2 = eval(subs(Br1_2,f,f1_2) + subs(Br2_2,f,f2_2));

    Bt2 = subs(Bt,Xi,Xi2);
    Bt1_2 = subs(Bt2,Bpole,Bpole_1);
    Bt1_2 = subs(Bt1_2,l,l_1);
    Bt2_2 = subs(Bt2,Bpole,Bpole_2);
    Bt2_2 = subs(Bt2_2,l,l_2);
    Bt2 = eval(subs(Bt1_2,g,g1_2) + subs(Bt2_2,g,g2_2));

    B2_mag = (Br2^2+Bt2^2)^0.5;

    %calculating change in r and theta
    dr1 = -Br1*ds/B1_mag;
    dt1 = -Bt1*ds/r1(j)/B1_mag;
    dr2 = Br2*ds/B2_mag;
```

```
    dt2 = Bt2*ds/r2(j)/B2_mag;

    %calculating new r and theta coords
    r1(j+1) = r1(j) + dr1;
    t1(j+1) = t1(j) + dt1;
    r2(j+1) = r2(j) + dr2;
    t2(j+1) = t2(j) + dt2;

    %checking if r is below R
    if r1(j+1) < R
        t1(j+1) = t1(j);
        r1(j+1) = R;
        tr1_check = 1;

        t1_footpoint(s) = t1(j+1);
        r1_footpoint(s) = r1(j+1);

        f1_1 = subs(Pl_1,X,t1_footpoint(s));
        g1_1 = subs(Plm_1,X,t1_footpoint(s));
        f2_1 = subs(Pl_2,X,t1_footpoint(s));
        g2_1 = subs(Plm_2,X,t1_footpoint(s));

        Br0 = subs(Br,Xi,r1_footpoint(s)/R);
        Br0_1 = subs(Br0,Bpole,Bpole_1);
        Br0_1 = subs(Br0_1,l,l_1);
        Br0_2 = subs(Br0,Bpole,Bpole_2);
        Br0_2 = subs(Br0_2,l,l_2);
        Br0 = eval(subs(Br0_1,f,f1_1) + subs(Br0_2,f,f2_1));

        Bt0 = subs(Bt,Xi,r1_footpoint(s)/R);
        Bt0_1 = subs(Bt0,Bpole,Bpole_1);
        Bt0_1 = subs(Bt0_1,l,l_1);
        Bt0_2 = subs(Bt0,Bpole,Bpole_2);
        Bt0_2 = subs(Bt0_2,l,l_2);
        Bt0 = eval(subs(Bt0_1,g,g1_1) + subs(Bt0_2,g,g2_1));

        p0_1 = k*(Br0^2+Bt0^2);
    end

    if r2(j+1) < R
       t2(j+1) = t2(j);
       r2(j+1) = R;
       tr2_check = 1;

       t2_footpoint(s) = t2(j+1);
```

```
        r2_footpoint(s) = r2(j+1);

        f1_2 = subs(Pl_1,X,t2_footpoint(s));
        g1_2 = subs(Plm_1,X,t2_footpoint(s));
        f2_2 = subs(Pl_2,X,t2_footpoint(s));
        g2_2 = subs(Plm_2,X,t2_footpoint(s));

        Br0 = subs(Br,Xi,r2_footpoint(s)/R);
        Br0_1 = subs(Br0,Bpole,Bpole_1);
        Br0_1 = subs(Br0_1,l,l_1);
        Br0_2 = subs(Br0,Bpole,Bpole_2);
        Br0_2 = subs(Br0_2,l,l_2);
        Br0 = eval(subs(Br0_1,f,f1_2) + subs(Br0_2,f,f2_2));

        Bt0 = subs(Bt,Xi,r2_footpoint(s)/R);
        Bt0_1 = subs(Bt0,Bpole,Bpole_1);
        Bt0_1 = subs(Bt0_1,l,l_1);
        Bt0_2 = subs(Bt0,Bpole,Bpole_2);
        Bt0_2 = subs(Bt0_2,l,l_2);
        Bt0 = eval(subs(Bt0_1,g,g1_2) + subs(Bt0_2,g,g2_2));

        p0_2 = k*(Br0^2+Bt0^2);
    end

    %checking if theta is in range of 0 to pi
    if t1(j+1) < 0
        t1(j+1) = 0;
        r1(j+1) = r1(j);
        tr1_check = 1;
        p0_1 = p0_2;
    end
    if t1(j+1) > pi/2
        t1(j+1) = pi/2;
        r1(j+1) = r1(j);
        tr1_check = 1;
        p0_1 = p0_2;
    end
    if t2(j+1) < 0
        t2(j+1) = 0;
        r2(j+1) = r2(j);
        tr2_check = 1;
        p0_2 = p0_1;
    end
    if t2(j+1) > pi/2
        t2(j+1) = pi/2;
```

```
            r2(j+1) = r2(j);
            tr2_check = 1;
            p0_2 = p0_1;
        end
        %breaking when field lines are complete
        if tr1_check == 1
            if tr2_check == 1
                break
            end
        end
    end

    iteration_counter = [iteration_counter,j];

    figure(1)

    B1 = zeros(1,n);%magnitude of B field strength
    B2 = zeros(1,n);
    B1(B1==0) = NaN;
    B2(B2==0) = NaN;

    for b = 1:j
        Xi1 = r1(b)/R;
        Xi2 = r2(b)/R;

        f1_1 = subs(Pl_1,X,t1(b));
        g1_1 = subs(Plm_1,X,t1(b));
        f1_2 = subs(Pl_1,X,t2(b));
        g1_2 = subs(Plm_1,X,t2(b));
        f2_1 = subs(Pl_2,X,t1(b));
        g2_1 = subs(Plm_2,X,t1(b));
        f2_2 = subs(Pl_2,X,t2(b));
        g2_2 = subs(Plm_2,X,t2(b));

        Br1 = subs(Br,Xi,Xi1);
        Br1_1 = subs(Br1,Bpole,Bpole_1);
        Br1_1 = subs(Br1_1,l,l_1);
        Br2_1 = subs(Br1,Bpole,Bpole_2);
        Br2_1 = subs(Br2_1,l,l_2);

        Br1 = eval(subs(Br1_1,f,f1_1) + subs(Br2_1,f,f2_1));

        Bt1 = subs(Bt,Xi,Xi1);
        Bt1_1 = subs(Bt1,Bpole,Bpole_1);
        Bt1_1 = subs(Bt1_1,l,l_1);
```

```
    Bt2_1 = subs(Bt1,Bpole,Bpole_2);
    Bt2_1 = subs(Bt2_1,l,l_2);

    Bt1 = eval(subs(Bt1_1,g,g1_1) + subs(Bt2_1,g,g2_1));

    B1(b) = (Br1^2+Bt1^2)^0.5;

    Br2 = subs(Br,Xi,Xi2);
    Br1_2 = subs(Br2,Bpole,Bpole_1);
    Br1_2 = subs(Br1_2,l,l_1);
    Br2_2 = subs(Br2,Bpole,Bpole_2);
    Br2_2 = subs(Br2_2,l,l_2);

    Br2 = eval(subs(Br1_2,f,f1_2) + subs(Br2_2,f,f2_2));

    Bt2 = subs(Bt,Xi,Xi2);
    Bt1_2 = subs(Bt2,Bpole,Bpole_1);
    Bt1_2 = subs(Bt1_2,l,l_1);
    Bt2_2 = subs(Bt2,Bpole,Bpole_2);
    Bt2_2 = subs(Bt2_2,l,l_2);

    Bt2 = eval(subs(Bt1_2,g,g1_2) + subs(Bt2_2,g,g2_2));

    B2(b) = (Br1^2+Bt1^2)^0.5;

    %magnetic pressure from field line calculation
    p_mag_1(b) = B1(b)^2/8/pi;
    p_mag_2(b) = B2(b)^2/8/pi;

    %gas pressure calculations
    J_2_1 = subs(J2,t,t1(b));
    J_2_1 = subs(J_2_1,Xi,Xi1);
    J_2_1 = eval(int(J_2_1,1,Xi1));

    J_2_2 = subs(J2,t,t2(b));
    J_2_2 = subs(J_2_2,Xi,Xi2);
    J_2_2 = eval(int(J_2_2,1,Xi2));

    J_3_1 = subs(J3,t,t1(b));
    J_3_1 = subs(J_3_1,Xi,Xi1);

    if and(Br1 < ds, Br1 > -ds) == 0
        BtBr1 = Bt1/Br1;
        J_3_1 = subs(J_3_1,BtBr,BtBr1);
        J_3_1 = eval(int(J_3_1,1,Xi1));
```

```
        p_gas_1(b) = p0_1*exp(phig*(1/Xi1-1)+phic*(J_2_1+J_3_1));
    else
        p_gas_1(b) = p0_1;
    end

    J_3_2 = subs(J3,t,t1(b));
    J_3_2 = subs(J_3_2,Xi,Xi2);

    if and(Br2 < ds, Br2 > -ds) == 0
        BtBr2 = Bt2/Br2;
        J_3_2 = subs(J_3_2,BtBr,BtBr2);
        J_3_2 = eval(int(J_3_2,1,Xi2));
        p_gas_2(b) = p0_2*exp(phig*(1/Xi2-1)+phic*(J_2_2+J_3_2));
    else
        p_gas_2(b) = p0_2;
    end

    if pcheck(s) ≠ 1
        p_gas_1(b)
        p_gas_2(b)
        B1(b)
        B2(b)
        if or(p_gas_1(b)/p_mag_1(b) ≥ 1,p_gas_2(b)/p_mag_2(b) ≥ 1) == 1
            if abs(rmax_temp(s)-rmax_max(s)) ≤ ds/10
                pcheck(s) = 1;
            elseif rmax_temp(s) == rmax_prev(s)
                pcheck(s) = 1;
            else
                pcheck(s) = 2;
                rmax_max(s) = rmax_temp(s);
                rmax_temp(s) = rmax_prev(s)
                break
            end
        elseif pcheck(s) == 2
            rmax_prev(s) = rmax_temp(s);
            rmax_temp(s) = (rmax_temp(s) + rmax_max(s))/2
            break
        end
    end

    if pcheck(s) == 1%if rmax has been found
        dr1grid = abs(diff([r1(b),r1(b+1)]));
        dr2grid = abs(diff([r2(b),r2(b+1)]));
        dtheta1grid = abs(diff([t1(b),t1(b+1)]));
        dtheta2grid = abs(diff([t2(b),t2(b+1)]));
```

```
        theta1grid = t1(b):dtheta1grid:S(s);
        theta2grid = t2(b):dtheta2grid:S(s);

        for i = 1:numel(theta1grid)
            V = V + abs(r1(b)^2*sin(theta1grid(i))*dtheta1grid*4*pi*dr1grid);
            E = E + ...
                abs(r1(b)^2*sin(theta1grid(i))*dtheta1grid*4*pi*dr1grid*p_gas_1(b)^2);
        end
        for i = 1:numel(theta2grid)
            V = V + abs(r2(b)^2*sin(theta2grid(i))*dtheta2grid*4*pi*dr2grid);
            E = E + ...
                abs(r2(b)^2*sin(theta2grid(i))*dtheta2grid*4*pi*dr2grid*p_gas_2(b)^2);
        end

%         figure(1)
%         ...
    plot([R*sin(t1(b)),r1(b)*sin(t1(b))],[R*cos(t1(b)),r1(b)*cos(t1(b))],'g')
%         ...
    plot([R*sin(t2(b)),r2(b)*sin(t2(b))],[R*cos(t2(b)),r2(b)*cos(t2(b))],'g')

    end
    %saving gas and magnetic pressure values for plot
    if t1(b) == pi/2
        p_gas_1_axis = [p_gas_1_axis,p_gas_1(b)];
        p_mag_1_axis = [p_mag_1_axis,p_mag_1(b)];
        rmax_axis = [rmax_axis,r1(b)];
    end
end

%calculating x and z coords
x1 = r1.*sin(t1);
z1 = r1.*cos(t1);
x2 = r2.*sin(t2);
z2 = r2.*cos(t2);
x1(x1==0)=NaN;%removing values equal to 0
z1(z1==0)=NaN;
x2(x2==0)=NaN;
z2(z2==0)=NaN;

if pcheck(s) == 1%if rmax has been found

    %combining data matrices for plots (dont work)
    t_max = [fliplr(t1),t2];
    B_max = [fliplr(B1),B2];
    r1(r1==0)=NaN;
```

```
    r2(r2==0)=NaN;
    r_max_r = [fliplr(r1),r2];

    %rmax plot
    figure(1)
    r_max = ...
       plot(ax,[x1,x2,x1,x2,-x1,-x2,-x1,-x2],[z1,z2,-z1,-z2,z1,z2,-z1,-z2],'-r','Displa

    %gas pressure and magnetic pressure plot
    figure(2)
    bx = gca;
    hold(bx,'on')
    beta_axis = p_gas_1_axis./p_mag_1_axis - 1;
    plot(rmax_axis,beta_axis,'r','DisplayName','\beta - 1')
    yline(0,'--')
    ylabel('\beta - 1')
    xlabel('r/R_*')
    title('\beta - 1 against \xi')%title
    hold(bx,'off')

    %Magnetic Field Strength plot
    figure(3)
    bx = gca;
    hold (bx,'on')
    plot(r_max_r,B_max,'b')
    ylabel('Magnetic Field Strength, B (Gauss)')
    xlabel('r/R_*')
    title('Magnitude of Magnetic Feild Strength With Distance From Stars ...
       Surface')%title
    hold(bx,'off')

    %breaking while loop once rmax has been plotted
    pcheck(s) = 3;
end
if pcheck(s) == 0%if normal closed field line
    plot(ax,[x1,x2,x1,x2,-x1,-x2,-x1,-x2],[z1,z2,-z1,-z2,z1,z2,-z1,-z2],'-b');
    figure(1)
    %calculate new rmax temp
    rmax_prev(s) = rmax_temp(s);
    rmax_temp(s) = rmax_temp(s)+1;
end
end
end

if 10^5.75 < T < 10^6.3
```

```
    AT = 10^-21.94;
elseif 10^6.3 < T < 10^7.3
    AT = 10^-17.73*T^(-2/3);
elseif T > 10^7.3
    AT = 10^-21.94*T^(1/4);
end

%in cubic stellar radii into cm **stellar radius cubed
Lx = AT*E*R_Star^3/4/k_B^2/T^2;

disp(['numeric volume ',num2str(V)]) %displaying volume value
% disp(['analytic volume ...
    ',num2str(4*pi/3*rmax_temp^3*2/35*(1-1/rmax_temp)^1.5*(8 + ...
    12/rmax_temp + 15/rmax_temp^2))])
disp(['numeric rmax ',num2str(rmax_temp)])
disp(['numeric x-ray luminosity Lx ',num2str(Lx)])

figure(1)
theta_star = linspace(0,2*pi,60);%linspace of theta values used to plot star
xstar = cos(theta_star)*R;%x coordinates of the star
zstar = sin(theta_star)*R;%z coordinates of the star
Star = plot(ax,xstar,zstar,'-k','Linewidth',2,'DisplayName','Star');
axis equal
axis([-(max(r_max_r)) (max(r_max_r)) -(max(r_max_r)) ...
    (max(r_max_r))])%setting axis
set(gca,'FontSize',16)
set(gcf,'color','w');
print(gcf,'field.png','-dpng','-r600');
hold (ax,'off')%showing graph
```

```
figure(1)
set(gca,'xtick',0:5)
ax = gca;
hold (ax,'on')
grid (ax,'on')
title(ax,'L_X vs Field Complexity')
xlabel(ax,'Field Configuration')
ylabel(ax,'log of X-ray Luminosity log(L_x)')
Lx = ...
    log10([1.268217346265914e+32,3.276328197219336e+31,1.3630589915108e+31,6.33146398238
l = [1,2,3,4];
plot(ax,l,Lx,'-or')
axis([0 5 min(Lx)-1 max(Lx)+1])
```

```
hold (ax,'off')

figure(2)
set(gca,'xtick',0:5)
ax = gca;
hold (ax,'on')
grid (ax,'on')
title(ax,'Enclosed Coronal Volume vs Field Complexity')
xlabel(ax,'Field Configuration')
ylabel(ax,'Enclosed Coronal Volume, cubed units')
V = [73.3476,13.9944,16.518,7.6217];
l = [1,2,3,4];
plot(ax,l,V,'-or')
axis([0 5 min(V)-1 max(V)+1])
hold (ax,'off')

figure(3)
set(gca,'xtick',0:5)
ax = gca;
hold (ax,'on')
grid (ax,'on')
title(ax,'r_{max} vs Field Complexity')
xlabel(ax,'Field Configuration')
ylabel(ax,'r_{max}, R_*')
rmax1 = [3.4209,2.4365,2.0269,1.7983];
rmax2 = [3.4209,2.4365,2.2534,1.9561];
l = [1,2,3,4];
plot(ax,l,rmax1,'-or')
plot(ax,l,rmax2,'-o')
axis([0 5 min(rmax)-1 max(rmax)+1])
hold (ax,'off')

figure(4)
set(gca,'xtick',0:5)
ax = gca;
hold (ax,'on')
grid (ax,'on')
title(ax,'L_X vs B_{oct}/B_{dip} Ratios')
xlabel(ax,'B_{oct}/B_{dip}')
ylabel(ax,'log of X-ray Luminosity log(L_x)')
Lx = ...
    log10([4.171954727226028e+33,8.615571055812381e+35,3.450738733270904e+33,1.590408234
l = [1,4/3,3,5];
plot(ax,l,Lx,'-or')
axis([0 5 min(Lx)-1 max(Lx)+1])
```

```
hold (ax,'off')

figure(5)
set(gca,'xtick',0:5)
ax = gca;
hold (ax,'on')
grid (ax,'on')
title(ax,'Volume vs B_{oct}/B_{dip} Ratios')
xlabel(ax,'B_{oct}/B_{dip}')
ylabel(ax,'Enclosed Coronal Volume, cubed units')
V = [248.0459,333.3477,22.8545,20.631];
l = [1,4/3,3,5];
plot(ax,l,V,'-or')
axis([0 5 min(V)-1 max(V)+1])
hold (ax,'off')

figure(6)
set(gca,'xtick',0:5)
ax = gca;
hold (ax,'on')
grid (ax,'on')
title(ax,'r_{max} vs B_{oct}/B_{dip} Ratios')
xlabel(ax,'B_{oct}/B_{dip}')
ylabel(ax,'r_{max}, R_*')
rmax1 = [3.2105,3.0576,2.6093,2.373];
rmax2 = [2.7508,2.5492,1.4483,1.7258];
l = [1,4/3,3,5];
plot(ax,l,rmax1,'-or')
plot(ax,l,rmax2,'-o')
axis([0 5 min(rmax)-1 max(rmax)+1])
hold (ax,'off'
```